JCB Journal of Cell Biology

ARTICLE

Stress granules display bistable dynamics modulated by Cdk

Galal Yahya[1,2*], Alexis P. Pérez[1,3*], Mònica B. Mendoza[1], Eva Parisi[1], David F. Moreno[1], Marta H. Artés[1], Carme Gallego[1], and Martí Aldea[1,3]

Stress granules (SGs) are conserved biomolecular condensates that originate in response to many stress conditions. These membraneless organelles contain nontranslating mRNAs and a diverse subproteome, but our knowledge of their regulation and functional relevance is still incipient. Here, we describe a mutual-inhibition interplay between SGs and Cdc28, the budding yeast Cdk. Among Cdc28 interactors acting as negative modulators of Start, we have identified Whi8, an RNA-binding protein that localizes to SGs and recruits the mRNA of *CLN3*, the most upstream G1 cyclin, for efficient translation inhibition and Cdk inactivation under stress. However, Whi8 also contributes to recruiting Cdc28 to SGs, where it acts to promote their dissolution. As predicted by a mutual-inhibition framework, the SG constitutes a bistable system that is modulated by Cdk. Since mammalian cells display a homologous mechanism, we propose that the opposing functions of specific mRNA-binding proteins and Cdk's subjugate SG dynamics to a conserved hysteretic switch.

Introduction

Phase separation of proteins and nucleic acids into condensates is emerging as a general mechanism for cellular compartmentalization without the requirement of surrounding membranes (Banani et al., 2017; Alberti and Dormann, 2019; Shin and Brangwynne, 2017). These biomolecular condensates are based on weak multivalent interactions among component molecules that are mobile and exchange with the adjoining medium and play essential roles in cell physiology as reaction crucibles, sequestration centers, or organizational hubs. In a dynamic environment, cells need to control phase separation to form or dissolve condensates as a function of spatial and temporal cues. Thus, the molecular mechanisms that modulate phase separation will be critical to understanding how cells use biomolecular condensates to execute and control a growing list of cellular processes (Alberti et al., 2019; Snead and Gladfelter, 2019; Bratek-Skicki et al., 2020).

Stress granules (SGs) are conserved cytoplasmic condensates that contain (1) pools of nontranslating mRNAs and (2) a variety of proteins, including translation initiation factors and RNA-binding proteins that form core stable substructures in SGs (Protter and Parker, 2016). Non-RNA-binding proteins such as posttranslational modification factors, and protein or RNA remodeling complexes, are recruited to SGs by protein–protein interactions often mediated by intrinsically disordered regions (IDRs) and modulate SG assembly and disassembly. However, a predominant role has been recently attributed to intermolecular RNA–RNA interactions as upstream determinants of SG composition (Van Treeck et al., 2018). Although SGs are thought to down-regulate translation and protect recruited mRNAs in many different stress conditions, we still do not have sufficient experimental evidence to comprehend the relevance of SGs in cell physiology.

Stress restricts cell cycle progression, and budding yeast cells display a diverse set of mechanisms as a function of the stress signal. The HOG pathway constitutes a prominent paradigm and operates on specific molecular targets to modulate different cell cycle phases and transitions in response to osmotic stress (Solé et al., 2015; de Nadal et al., 2011). Regarding entry into the cell cycle, osmotic shock causes a temporary repression of the G1/S regulon (Bellí et al., 2001), in which Hog1-mediated phosphorylation of Whi5 and Msa1 contributes to inhibiting transcription (González-Novo et al., 2015). Down-regulation of G1/S genes was also observed during heat and ER stress (Rowley et al., 1993; Vai et al., 1987), and because chaperones play important but limiting roles at Start (Vergés et al., 2007; Yahya et al., 2014; Parisi et al., 2018), we proposed that, by compromising chaperone availability, all stressful conditions would target the chaperone as a common means to hinder entry into the cell cycle (Moreno et al., 2019). However, the precise molecular environment in which diverse

[1]Molecular Biology Institute of Barcelona, Spanish National Research Council, Catalonia, Spain; [2]Department of Microbiology and Immunology, Zagazig University, Zagazig, Egypt; [3]Department of Basic Sciences, Universitat Internacional de Catalunya, Barcelona, Spain.

*G. Yahya and A.P. Pérez contributed equally to this paper; Correspondence to Carme Gallego: carme.gallego@ibmb.csic.es; Martí Aldea: marti.aldea@ibmb.csic.es.

stress conditions would converge to modulate Start is still unknown.

Here, we describe the interplay between a common actor in stress, SGs, and the budding yeast Cdk, Cdc28. In a screen for Cdc28 interactors acting as negative modulators of Start, we identified Whi8, a putative RNA-binding protein previously localized to SGs. Whi8 is important for recruiting the mRNA of *CLN3*, the most upstream G1 cyclin, to SGs and contributes to inhibiting its translation under stress conditions. On the other hand, Whi8-dependent recruitment of Cdc28 is important for timely dissolution of SGs when stress conditions are relieved. We also identified the key elements of a homologue mechanism in mammalian cells, and we propose that Cdk's create a conserved bistable system that regulates SG dynamics.

Results

Whi8 is a Cdc28 interactor that hinders cell cycle entry

We previously identified and characterized a $Cdc28^{wee}$ mutant that produces premature entry into the cell cycle, causing a small-cell-size phenotype, and to uncover new negative modulators of Start, we used quantitative proteomics to compare the interactomes of WT and wee Cdc28 proteins (Yahya et al., 2014; Fig. 1 A). The $Cdc28^{wee}$ mutant was expressed at similar levels to the WT Cdc28 protein but showed impaired retention at the ER and caused premature accumulation of the Cln3 cyclin in the nucleus (Yahya et al., 2014). The five aa substitutions in the $Cdc28^{wee}$ mutant are found clustered in the C-terminal lobe of Cdc28, far from the cyclin-binding region and the kinase cleft, and mostly affect basic amino acids with likely exposed side chains, suggesting that the $Cdc28^{wee}$ mutant has altered interaction properties with negative regulators of the yeast Cdk. Among the group of proteins displaying a lower binding to $Cdc28^{wee}$, we found YGR250c, a putative RNA-binding protein that has been localized to SGs (Buchan et al., 2008) and recently isolated as a multicopy suppressor of ER–mitochondria tethering complex defects (Kojima et al., 2016). To ascertain its role as a negative regulator of the yeast Cdk at Start, we measured the budding volume of cells lacking YGR250c, and found a clear reduction that strictly required the presence of Cln3, the most upstream G1 cyclin (Fig. 1 B). Since overexpression of YGR250c produced the opposite effect and increased the budding volume by nearly 50%, we named YGR250c as Whi8, following the nomenclature of genes modulating cell size at Start.

As expected, Whi8 levels were lower in $Cdc28^{wee}$ immunoprecipitates (IPs) compared with WT Cdc28 (Fig. 1 C), suggesting that the negative role of Whi8 at Start is mediated by physical interaction with the Cdc28 kinase. Notably, a bioinformatics analysis of 480 Cdc28 interacting proteins pinpointed Whi8 as the only gene product that (1) displays RNA-binding motifs, (2) is induced by heat shock, and (3) is present in SGs (Fig. 1 D). In all, Whi8 emerged as a putative mediator of SG-born signals restraining entry into the cell cycle.

Whi8 binds and recruits the *CLN3* mRNA to SGs

Since *cln3* was totally epistatic to the loss of Whi8 with regards to the cell size phenotype, we wanted to test whether the role of Whi8 at Start would be exerted on *CLN3*, perhaps due to its RNA-binding properties. We found that the *CLN3* mRNA was enriched 10-fold in Whi8 IPs (Fig. 2 A), thus displaying a similar behavior to Whi3, a protein previously shown to bind the *CLN3* mRNA and regulate cell cycle entry (Garí et al., 2001; Colomina et al., 2008). Supporting shared roles in modulating *CLN3* expression by their RNA-binding motifs, Whi8 and Whi3 were found to coimmunoprecipitate in an RNA-dependent manner (Fig. 2 B). By contrast, the interaction between Whi8 and Pub1, a component of SGs, did not depend on RNA (Fig. 2 C).

The *CLN3* mRNA was clearly enriched in Pub1 pull-downs in stressed cells (Fig. 2 D), which, considering the abovementioned interactions, suggested that Pub1 could recruit the *CLN3* mRNA to SGs through Whi8. In agreement with this idea, enrichment of the *CLN3* mRNA in Pub1 pull-downs was strongly diminished in *whi8* cells and totally abrogated in double *whi8 whi3* cells under stress conditions (Fig. 2 D). We next tested whether the *CLN3* mRNA colocalized with Whi8 in SGs using the MS2v6 system (Tutucci et al., 2018). We observed some autofluorescent foci in control cells under stress, but they were in much lower numbers per cell compared with those produced by MCP-NLS-2GFP in the presence of the *CLN3-MS2v6* mRNA (Fig. S1 A), which did not form foci in the absence of stress (Fig. 2 E). As already described (Buchan et al., 2008), Whi8-GFP readily formed bright granules in the cytoplasm under stress conditions, where the *CLN3* mRNA readily colocalized (Fig. 2 E). Although the *CLN3* mRNA was previously found in SGs with Whi3 (Holmes et al., 2013; Cai and Futcher, 2013), the presence of Whi3 was totally dispensable. We found that colocalization of the *CLN3* mRNA with Pub1-mCherry granules required Whi8 and, to a much lesser extent, Whi3 (Figs. 2 F and S1 B), which gives further support to the notion that the *CLN3* transcript is recruited to SGs with the essential role of Whi8.

Whi8 is recruited to SGs via an IDR and is required to inhibit *CLN3* mRNA translation under stress conditions

Whi8 contains a C-terminal region of 120 residues largely dominated by disorder-prone amino acids (Fig. 3 A), suggesting that Whi8 could be recruited to SGs by an IDR. Deletion of these amino acids did not have any noticeable effect on cell size under normal growing conditions, but Whi8-ΔIDR was completely absent in the ER fractions as compared with the WT protein (Fig. 3 B). Moreover, although Whi8-ΔIDR was still recruited to SGs under stress conditions, the number of foci per cell and the fraction of Whi8-ΔIDR in SGs were sharply reduced (Fig. 3, C–F).

One of the hallmarks of SG-recruited mRNAs is translation inhibition, which, particularly for short-lived proteins such as Cln3, may have important effects in the corresponding downstream processes. We found that Cln3 levels rapidly decreased under stress conditions (Fig. S2 A), reaching a fivefold reduction in less than 30 min, while the *CLN3* mRNA was only reduced by 40% compared with unstressed cells (Fig. S2 C). Notably, levels of Cln3 decreased very slowly in cells lacking Whi8 (Fig. S2 A), thus reinforcing the notion that Whi8 would recruit the *CLN3* mRNA to SGs to inhibit its translation under stress conditions. Overexpression of SG components promotes SG formation and recapitulates inhibition of SG-reporter gene expression in

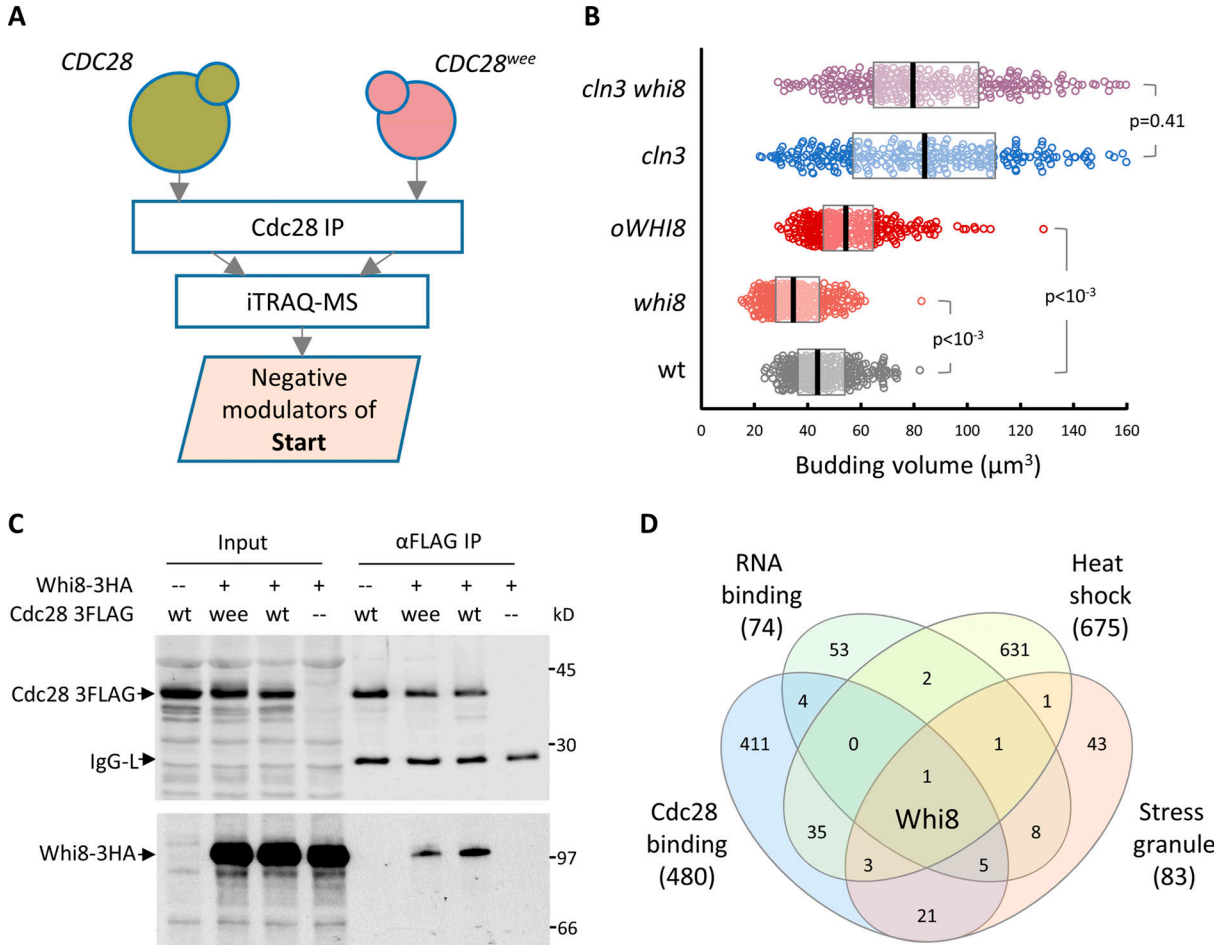

Figure 1. **Whi8 is a Cdc28 interactor that hinders cell cycle entry. (A)** Schematic of the screen for Cdc28 interactors as negative regulators of Start (Yahya et al., 2014). Briefly, pull-downs of WT and *wee* Cdc28 were analyzed by isobaric tags for relative and absolute quantitation and mass spectrometry (iTRAQ-MS) to identify proteins with a reduced affinity for Cdc28^{wee}. **(B)** Cells with the indicated genotypes were analyzed to determine cell size at budding. Individual data (n > 300) and median ± Q values are plotted. Shown P values were obtained using a Mann–Whitney U test. **(C)** Immunoblot of input and αFLAG immunoprecipitation samples from *WHI8-3HA* cells with plasmids expressing WT or mutant (*wee*) Cdc28-3FLAG proteins. **(D)** Venn diagram showing the overlapping of proteins that are (1) physical interactors of Cdc28, (2) contain demonstrated or putative RNA-binding domains, (3) are up-regulated by heat shock, and (4) were identified as SG components. wt, wild type.

nonstressed cells (Kedersha and Anderson, 2007). Accordingly, when we overexpressed Whi8 in the absence of stress, we observed a significant decrease in Cln3 protein levels (Fig. S2 B), while mRNA levels remained unchanged (Fig. S2 C). Whi8 overexpression did not induce SG formation, suggesting that Whi8 would have a direct effect on *CLN3* mRNA translation. Similarly to Whi3 (Wang et al., 2004) and Whi7 (Yahya et al., 2014), loss or overexpression of Whi8 increased or decreased, respectively, the nuclear levels of Cln3 (Fig. S2 D). These data explain the observed large cell size phenotype of Whi8-overexpressing cells and emphasize the idea that Whi8 acts as a negative regulator of Start by modulating expression of the *CLN3* mRNA.

Cdc28 is recruited to SGs and modulates SG dynamics

Cdc28 has been colocalized with Pbp1 in foci of stationary-phase cells (Shah et al., 2014), and, although not quantitative, a proteomic survey reported the presence of Cdc28 in SGs (Jain et al., 2016). To ascertain this possibility, we analyzed Cdc28-GFP and Pub1-mCherry in live cells under stress conditions and found that both proteins displayed extensive colocalization patterns (Fig. 4 A). Careful measurement of the relative levels of the two proteins in SGs yielded a steeper slope when Cdc28-GFP was taken as a dependent variable (Fig. 4 B), favoring Pub1 as an upstream factor for Cdc28 localization to SGs. Notably, the ratio of Cdc28-GFP to Pub1-mCherry in SGs decreased to ∼40% when comparing *whi8* with WT cells (Figs. 4 C and S3 A). Similarly to other components of the SG (Youn et al., 2018), Cdc28 and Pub1 were found to coimmunoprecipitate under nonstress conditions (Fig. 4 D). In all, these data underscore the relevance of Whi8 and Pub1 in recruiting Cdc28 to SGs.

A significant number of SG proteins (Jain et al., 2016) may be phosphorylation targets of Cdc28 (Fig. 4 E), and, in addition to Whi8, we found several translation initiation factors that are thought to be involved in translational repression in SGs (Table S1). This observation led us to hypothesize that Cdc28 could play a role in SG assembly and dissolution. To test this possibility, we carefully measured the dissolution kinetics of Pub1-mCherry

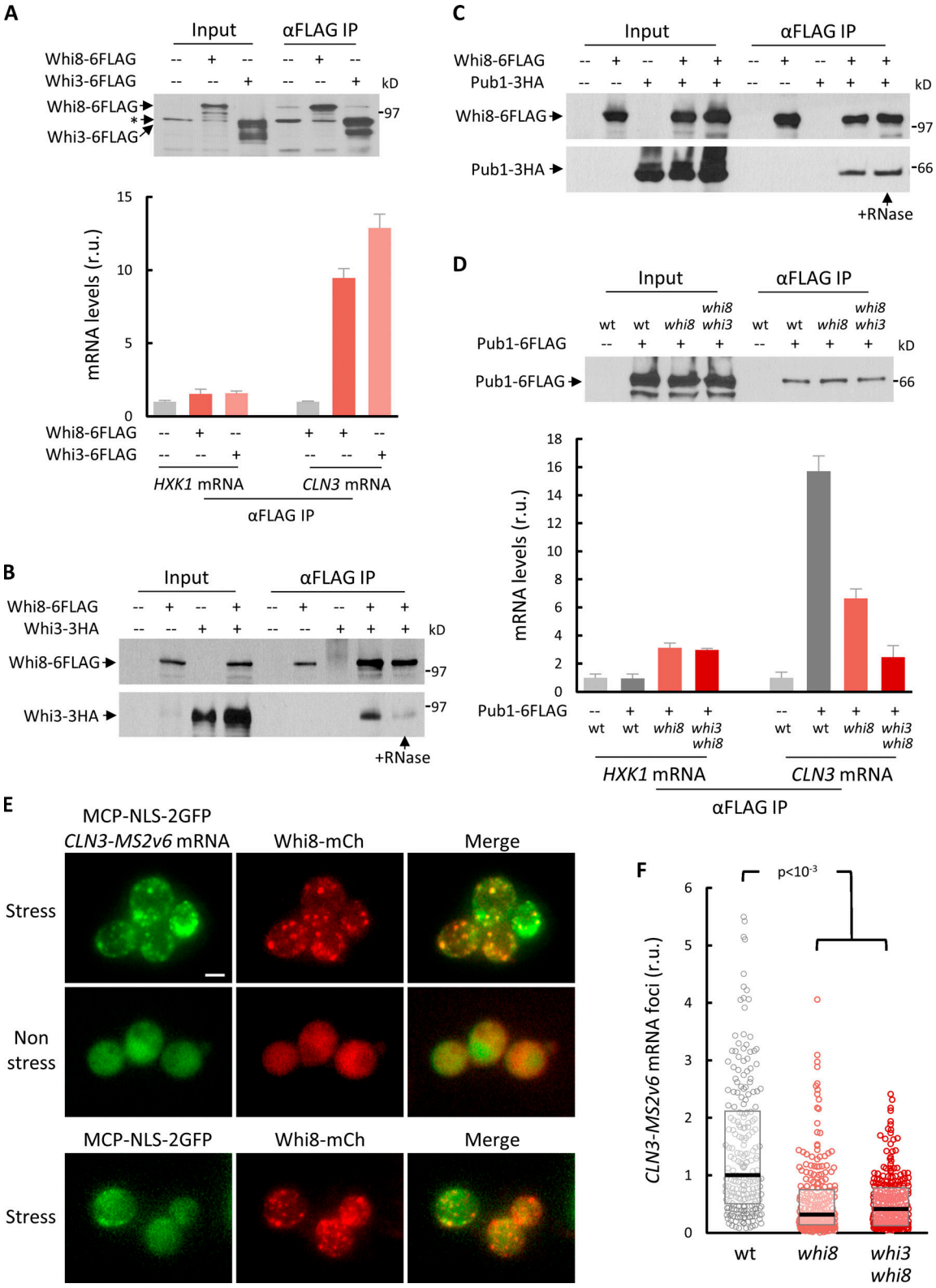

Figure 2. **Whi8 binds and recruits the *CLN3* mRNA to SGs. (A)** Immunoblot of input and αFLAG IPs from *WHI8-6FLAG*, *WHI3-6FLAG* or untagged cells (top). Levels of *CLN3* and *HXK1* (as control) mRNAs in IPs were determined in relative units (r.u.), and mean + SEM values (n = 3) are plotted (bottom). **(B and C)** Immunoblots of input and αFLAG IPs from cells expressing the indicated proteins. RNase was added during immunoprecipitation when indicated. **(D)** WT, *whi8*, or double *whi8 whi3* mutant cells expressing Pub1-6FLAG were stressed at 42°C for 30 min in the absence of glucose. An immunoblot of input and αFLAG IPs is shown at the top. Levels of *CLN3* and *HXK1* (as control) mRNAs were determined, and mean + SEM values (n = 3) are plotted (bottom). **(E)** *WHI8-mCh* cells with plasmids expressing *CLN3-MS2v6 and MCP-NLS-2GFP* after 30 min at 42°C in the absence of glucose (top). Nonstressed (center) and stressed *CLN3* control (bottom) cells are also shown. Scale bar, 2 µm. **(F)** *PUB1-mCh* cells with the indicated genotypes with plasmids expressing *CLN3-MS2v6* and *MCP-NLS-2GFP* were stressed as above, and the number of MCP-NLS-2GFP foci was measured. Individual data (n > 250) and median ± Q values are plotted. Shown P values were obtained using a Mann–Whitney U test. wt, wild type.

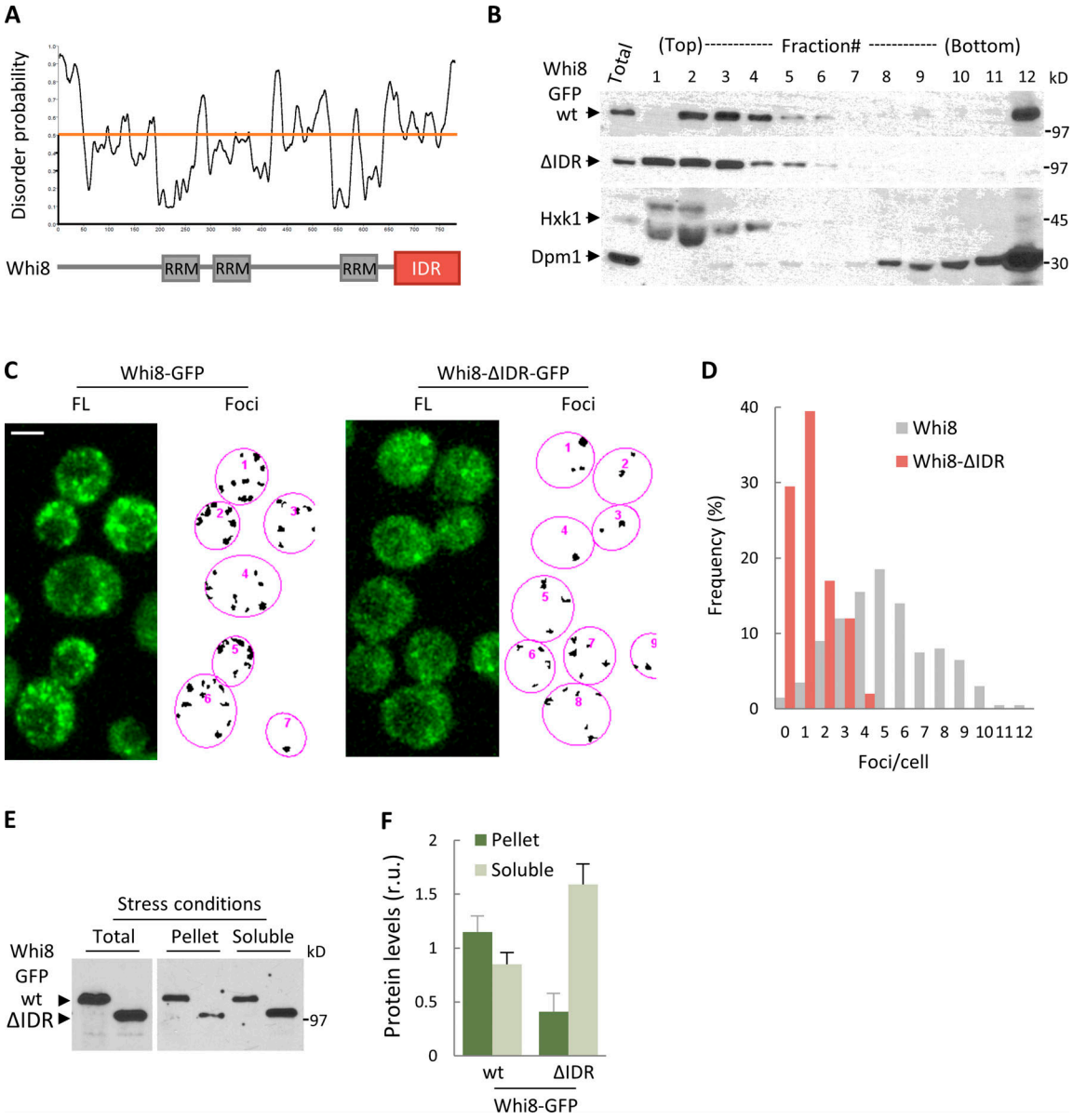

Figure 3. **Whi8 contains an IDR important for SG recruitment. (A)** Disorder probability of Whi8 amino acids and predicted RNA-recognition motifs and IDR. **(B)** Immunoblot analysis of the distribution of WT and ΔIDR Whi8-GFP in sucrose gradients. Hxk1 and Dpm1 are shown as soluble and ER markers, respectively. **(C)** Maximum projections of confocal fluorescence (FL) images from cells expressing WT and ΔIDR Whi8-GFP after 30 min at 42°C in the absence of glucose. Scale bar, 2 µm. Foci detected above a fixed local threshold with the aid of BudJ are also shown. **(D)** Cells expressing WT and ΔIDR Whi8-GFP were treated at 42°C in the absence of glucose and analyzed as in Fig. 4 A. Foci frequencies per cell are plotted (n = 200). **(E)** Immunoblot of WT and ΔIDR Whi8-GFP in the indicated fractions from cells as in D. **(F)** Whi8-GFP levels as in E were quantified, and mean + SEM values (n = 3) are plotted in relative units (r.u.). wt, wild type.

foci by time-lapse microscopy, and first compared cells carrying WT *CDC28* and thermosensitive *cdc28-13* alleles. Glucose was added to induce release from stress, but the temperature was only decreased to 37°C to maintain a restrictive scenario for the *cdc28-13* allele. As shown in Fig. 4 F, WT cells readily dissolved SGs under these partial-release conditions, and the levels of Pub1-mCherry in SGs decreased to 50% in only 21 min. By contrast, SG dissolution was much slower in *cdc28-13* cells, taking longer than 60 min to reach a 50% reduction in Pub1-mCherry in SGs (Fig. 4 F). As an independent approach, we used a G1-cyclin conditional strain that lacks Cln1,2 and holds Cln3 under the control of a regulatable promoter, which causes cells to arrest in G1 with no Cdk activity under repression conditions. We found a strikingly similar delay in SG dissolution when comparing G1-arrested and cycling cells (Fig. 4 G), which confirms the key role of Cdk activity in SG dissolution. Giving further support to this notion, cycling WT cells displayed clear differences in SG-dissolution kinetics depending on cell cycle position, being slower when Cdk activity is lower (i.e., G1 phase; Fig. S3 B). Finally, overexpression of Cln3 produced the opposite effects and reduced by 30% the half-life of SGs after release form stress (Fig. 4 F). Albeit surprisingly, the presence of *CLN3-1*, a

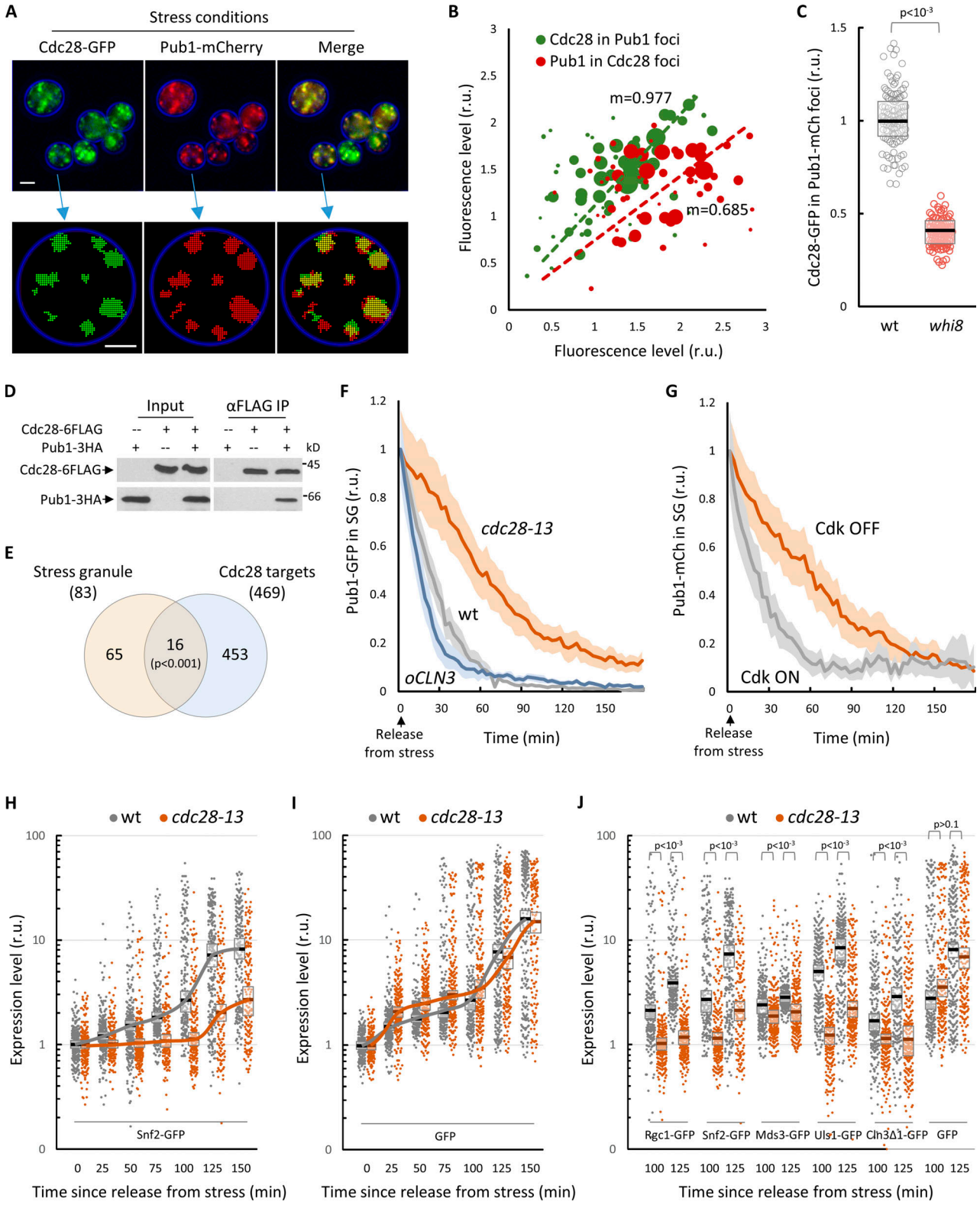

Figure 4. **Cdc28 is recruited to SGs and modulates SG dynamics. (A)** Maximum projections of confocal images from cells expressing Cdc8-GFP and Pub1-mCherry after 30 min at 42°C in the absence of glucose (top). Scale bar, 2 µm. GFP and mCherry foci detected for quantification in a sample cell with the aid of BudJ are also shown at the bottom (scale bar, 1 µm). **(B)** Cdc8-GFP levels in Pub1-mCherry foci (n = 60), and vice versa, from cells as in A are plotted in relative units (r.u.) with point diameter corresponding to foci size. Slope (m) values are also shown. **(C)** Cdc8-GFP levels in Pub1-mCherry foci were measured in WT and *whi8* cells stressed for 30 min at 42°C in the absence of glucose. Individual data (n = 125) and median ± Q values are plotted. Shown P value was obtained using a Mann–Whitney *U* test. **(D)** Immunoblot of input and αFLAG immunoprecipitation samples from cells expressing Cdc28-6FLAG and Pub1-3HA. **(E)** Venn diagram showing the overlapping of proteins that (1) were identified as SG components and (2) are putative phosphorylation targets of Cdc28. The indicated P

value was obtained assuming completely independent allocations. **(F)** WT, *cdc28-13*, and *oCLN3* (*tetO$_2$-CLN3*) cells expressing Pub1-mCherry were stressed for 30 min at 42°C in the absence of glucose, and, once released at 37°C in the presence of glucose, Pub1-mCherry levels in foci were measured at different time points. Mean values (n > 30) and confidence limits for the mean (α = 0.05) are plotted. **(G)** *GAL1p-CLN3 cln1,2* cells expressing Pub1-mCherry were grown in galactose and arrested in G1 by transfer to glucose for 2 h (Cdk OFF). Cells were then stressed for 30 min at 42°C in the absence of glucose, and, once released at 30°C in the presence of glucose to maintain the G1 arrest, Pub1-mCherry levels in foci were measured at different time points. As control, *CLN3 cln1,2* cells (Cdk ON) were subjected to the same experimental conditions. Mean values (n > 30) and confidence limits for the mean (α = 0.05) are plotted. **(H and I)** WT (gray) and *cdc28-13* (orange) cells expressing the Gal4-hER-VP16 transactivator and plasmid-borne *SNF2-GFP* (H) or GFP (I) from the *GAL1p* promoter were added estradiol and immediately treated for 30 min at 42°C in the absence of glucose. Once released at 30°C in the presence of glucose, estradiol was removed to limit further accumulation of the *SNF2-GFP* mRNA. Single-cell fluorescence levels at the indicated time points are plotted. Median values (n > 200) and confidence limits for the median (α = 0.05) are also shown. **(J)** WT (gray) and *cdc28-13* (orange) cells with plasmids expressing the indicated GFP fusions from the *GAL1p* promoter were analyzed as in H. Single-cell fluorescence levels at the indicated time points after release from stress are plotted in relative units (r.u.). Median values (n > 200) and confidence limits for the median (α = 0.05) are also plotted. Shown P values were obtained using a Mann–Whitney U test. wt, wild type.

truncated hyperstable allele that reproduces most phenotypes of *CLN3* overexpression, was much less effective in SG dissolution (Fig. S3 C). Cln3-1 lacks a putative 91-aa IDR that could play additional roles in recruiting the Cdc28/Cln3 complex to SGs.

Our data point to the notion that Cdc28 boosts SG dissolution when cells are released from stress. Thus, we tested whether translation of SG-recruited mRNAs also depended on Cdk activity during release from stress. First, we selected four highly expressed mRNAs known to accumulate in SGs (Khong et al., 2017) that contain ORFs in the range of 1 to 6 kb and code for proteins readily detectable in the cytoplasm or the nucleus when fused to GFP (Huh et al., 2003): *SNF2*, *RGC1*, *MDS3*, and *ULS1*. As a paradigmatic example of a highly translated transcript (Siwiak and Zielenkiewicz, 2010), we first analyzed the *SNF2* mRNA. Expression of a C-terminal fusion of Snf2 to GFP under the *GAL1* promoter was induced with estradiol immediately after cells were subjected to stress. After 30 min, cells were placed under normal growth conditions in the absence of estradiol to limit further mRNA accumulation, and fluorescence levels were measured at different times during and after release from stress. In agreement with the fact that overall translation is rapidly inhibited (Crawford and Pavitt, 2019), Snf2-GFP fluorescence did not change significantly (P = 0.17) during stress and gradually increased up to eightfold when WT cells were returned to normal conditions (Fig. 4 H). Notably, whereas *SNF2-GFP* mRNA levels in WT and *cdc28-13* cells were comparable during recovery from stress (Fig. S3 D), Snf2-GFP fluorescence levels were much lower in *cdc28-13* cells and reached only a 2.5-fold increase at the final time point. We used free GFP as control and observed no significant differences in fluorescence increase when comparing WT and *cdc28-13* cells (Figs. 4 I and S3 D). Finally, we also analyzed other SG-recruited mRNAs such as *RGC1*, *MDS3*, *ULS1*, and *CLN3Δ1*, a hyperstable truncated allele that allows detection of the GFP fusion, and observed a Cdc28-dependent resumption of translation similar to that of *SNF2* (Figs. 4 J and S3 D). In all, these data demonstrate the important role of the Cdk in relieving translation inhibition of SG-recruited mRNAs and suggest a cause–effect relationship between SG dissolution and translation resumption.

Mammalian SGs contain Cdk-cyclin factors and are modulated by cell cycle position

SGs from yeast and mammalian cells display a highly significant overlap in composition and share distinct substructural traits (Jain et al., 2016). Thus, we anticipated that our findings in yeast cells would also apply to mammalian SGs. To test whether G1 cyclin mRNAs are recruited to mammalian SGs, we used the MS2-based approach and observed a clear colocalization of a *CCND1-MS2* mRNA with TIA1, the Pub1 mammalian homologue, in SGs of HeLa cells (Fig. S4 A). Caprin1, a component of SGs, binds the cyclin D2 mRNA in nonstressed 293T cells (Solomon et al., 2007). Thus, we tested whether Caprin1 would play a role in recruiting the cyclin D1 mRNA to SGs. First, we found that Caprin1 and the *CCND1-MS2* mRNA colocalized in SGs (Fig. 5 A). Interestingly, shRNA-driven down-regulation of Caprin1 levels was accompanied by a reduction in the number of foci produced by the *CCND1-MS2* mRNA under stress conditions (Fig. 5 B). SG formation, as assessed by TIA1 immunofluorescence, was not significantly affected in HeLa cells (Fig. S4 B). However, Caprin down-regulation has been shown to decrease the number of SGs in arsenite-treated U2OS cells (Kedersha et al., 2016). This discrepancy may be due to the different cell lines or, alternatively, to the fact that Caprin1 knockdown in our experiments was not as effective as that obtained in U2OS cells (Kedersha et al., 2016). In any event, even considering that SG number is not strongly affected in HeLa cells, the decrease levels of Caprin1 could also affect the ability of SG to recruit other proteins. In all, our data suggest that Caprin1 plays a direct or indirect role in *CCND1* mRNA recruitment to SGs, thus acting as a functional homologue of Whi8 in mammalian cells, where cyclin D1 protein levels are also strongly down-regulated during SGs formation (Fig. S4 C).

Next, we decided to test whether Caprin1 and Cdk4, a G1 Cdk, interact by coimmunoprecipitation as in yeast cells and found that these proteins are bound in a stress-dependent manner in HeLa cells (Fig. 5 C). Moreover, we observed almost overlapping patterns of localization of Caprin1 and Cdk4 in SGs (Fig. 5 D).

The rate of SG dissolution has been shown to be strongly diminished by Cdk inhibitors in HeLa and U2OS cells (Wippich et al., 2013). Hence, the presence of a G1 Cdk and the Caprin1-mediated recruitment of a G1 cyclin mRNA in SGs suggested that cell cycle progression could also play a role in SG dynamics in mammalian cells. As in yeast cells, Cdk activity is low in G1, suddenly increases during the G1/S transition, and becomes maximal during mitosis until anaphase. Using an mCherry-G3BP1 reporter to analyze SG-dissolution kinetics in U2OS cells expressing a mVenus-Gem$^{1-110}$ fusion that is stable from S phase to anaphase, we found that SG half-life was reduced by

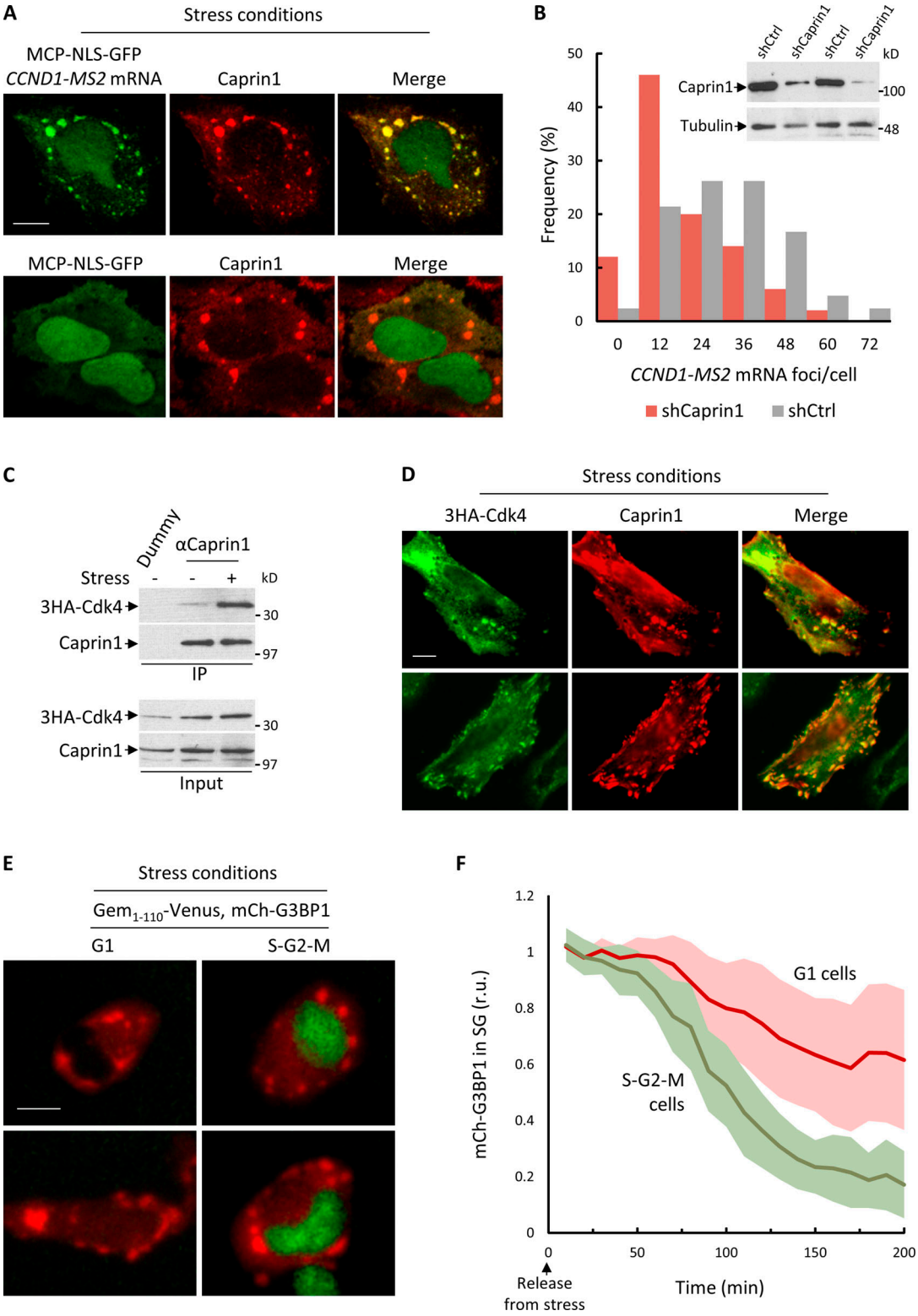

Figure 5. **Mammalian SGs contain Cdk-cyclin factors and are modulated by cell cycle position. (A)** HeLa cells with plasmids expressing NLS-MCP-GFP and either a *CCND1-MS2* mRNA or none (as control) were subjected to 0.5 mM $NaAsO_2$ for 30 min and analyzed by immunofluorescence with a αCaprin1 antibody. Scale bar, 5 µm. **(B)** HeLa cells with plasmids expressing NLS-MCP-GFP, a *CCND1-MS2* mRNA, and either shCaprin1 or shCtrl were subjected to 0.5 mM $NaAsO_2$ for 30 min and analyzed as in Fig. 4 A. Foci frequencies per cell (n = 40) are plotted. Inset: Immunoblot analysis of Caprin1 levels in total extracts of HeLa cells expressing shCaprin1 or shCtrl. Tubulin serves as loading control. **(C)** Immunoblot of input and αCaprin1 immunoprecipitation samples from HeLa cells with a plasmid expressing 3HA-Cdk4 in the presence (+) or absence (–) of 0.5 mM $NaAsO_2$ for 30 min. **(D)** HeLa cells expressing 3HA-Cdk4 were subjected to 0.5 mM $NaAsO_2$ for 30 min and analyzed by immunofluorescence with αHA and αCaprin1 antibodies. Scale bar, 5 µm. **(E)** Representative images of U2OS cells with plasmids expressing Geminin$_{1–110}$-mVenus and mCherry-G3BP1 after treatment with 0.5 mM $NaAsO_2$ for 30 min. Scale bar, 5 µm. **(F)** U2OS cells expressing Geminin$_{1–110}$-mVenus and mCherry-G3BP1 were treated with 0.5 mM $NaAsO_2$ for 30 min as in E, and, once released in fresh medium, mCherry-G3BP1 levels in foci were measured at different time points. Mean values (n = 25) and confidence limits for the mean (α = 0.05) are plotted.

twofold in cells progressing through S-G2-M phases, when Cdk activity is high, compared with G1 cells (Fig. 5, E and F). These data confirm our findings in yeast cells and point to the notion that SGs would antagonize Cdk activity by restraining cyclin translation under stress conditions and that, in turn, Cdk would accelerate SGs dissolution during release from stress.

Mutual inhibition as a bistable system for SG dynamics

To gain insight into the relevance of the counteracting effects between SGs and Cdk activity, we modeled SG dynamics in a mutual-inhibition system with Cdk (Figs. 6 A and S5 A). Briefly, we assumed that active Cdk (Cdk_{Cyc}) would act as an enzyme with specific catalytic (k_c) and Michaelis–Menten (K_M) constants to promote dissolution of SG factors (SG) as free components (SG_{Comp}). All other processes were defined by simple mass-action laws with explicit rate constants. We tried to keep the model as simple as possible in order to obtain all the kinetic parameters from experimental data. The K_M for Cdc28 was previously determined in vitro (Bouchoux and Uhlmann, 2011), and the maximal substrate concentration in SGs was estimated as described in Fig. S5 B. We obtained the basal SG-dissolution rate constant (k_{bd}) by fitting the model to SG dissolution in the *cdc28-13* mutant in the absence of stress (Fig. S5 C), where all other variables have no effect. We then used SG formation and dissolution data from WT cells to estimate the remaining rate constants (Fig. S5 D). With these experimental parameters, the mutual-inhibition model predicted a bistable switch as a function of the stress signal (Fig. 6 B). To observe how the bistability of the model arises, in Fig. 6 C we plotted the steady-state levels of condensed SG factors (SG) and active Cdk (Cdk_{Cyc}) as independently predicted by each of the two modules of the system, either (1) SG dissolution as a function of Cdk_{Cyc} and the stress level ($Stress$) or (2) Cdk_{Cyc} inactivation as a function of SG. At low stress, SG dissolution and Cdk_{Cyc} inactivation curves intersect only once and the system is monostable, with high active Cdk1 and low condensed SG factors. When stress reaches a certain value, the system creates a saddle-node bifurcation and a new stable steady-state, with low active Cdk1 and high levels of condensed SG factors. At higher stress levels, the SG-dissolution curve is pushed further and the system becomes monostable again, with low active Cdk1 and high SG condensation (Fig. 6 C). The relative K_M, which incorporates SG component concentration, has strong effects on the predicted bistability (Fig. 6 D), thus highlighting the importance of substrate accumulation in the SG itself to attain a bistable system.

We then tested whether SG steady states followed a pattern compatible with bistability as a function of stress. As a tunable stress effector, we used NaN_3 at different concentrations and measured SG formation after 1 h of treatment. We found that steady-state SG levels increased with stressor concentration following bistable kinetics and displayed a hysteretic behavior as predicted by the model when stressor concentration was reversed (Fig. 6, E and F). Finally, we used the G1-cyclin conditional strain to test the effects of Cdk activity in the switch-like behavior of SG formation as a function of NaN_3 concentration. Although a sigmoidal curve was still observed, G1-arrested cells with no Cdk activity advanced SG formation at lower stress levels in a similar fashion to what the model predicts if kinase levels are decreased (Fig. 6, G and H). These data support the important role of Cdk in SG dynamics and suggest that other kinases or factors important for SG formation and dissolution also act in mutual-inhibition modules.

Discussion

Here, we identified Whi8 (YGR250C) as a protein that interacts with the Cdc28 Cdk and recruits the *CLN3* cyclin mRNA to SGs for translational repression and, hence, Cdc28 inactivation under stress conditions in G1 cells. Moreover, the yeast Cdk is also recruited to SGs with the important participation of Whi8 and plays a crucial role in SG dissolution and translation resumption of SG-recruited mRNAs when cells are returned to nonstress conditions. We found a similar scenario in mammalian cells, where the *CCND1* cyclin mRNA is translationally repressed by stress and recruited to SGs with the contribution of Caprin1, an RNA-binding protein that interacts with Cdk4, a G1 Cdk, in a stress-dependent manner. While Cdk4 colocalizes with Caprin1 in SGs, SG dissolution is slower in cells where Cdk activity is lower (i.e., G1 cells) when released from stress conditions. Thus, Whi8 and Caprin1 would act as molecular links between Cdk inactivation and Cdk-dependent SG dissolution during adaptation to and recovery from stress, respectively. Finally, our data show that SGs behave as a Cdk-dependent bistable system that only switches when stress levels reach a minimal threshold or normal conditions are almost completely restored.

Recent work analyzed the presence of mRNAs in yeast SGs (Khong et al., 2017) and found that G1 cyclin mRNAs were enriched in the SG fraction (fourfold for *CLN3* and about twofold for *CLN1,2*), but levels of G1 cyclin mRNAs were still significant in the soluble fraction. Moreover, similar data from mammalian cells showed no or only a modest enrichment of *CCND1,2,3* mRNAs in SGs (Khong et al., 2017; Namkoong et al., 2018). Thus, although recruitment to SGs likely plays an important role, other mechanisms such as eIF2α inhibition by phosphorylation (Crawford and Pavitt, 2019) could act to ensure full inhibition of translation of G1 cyclin mRNAs under stress conditions. On the other hand, recruitment of a fraction of cyclin mRNAs to SGs could increase local Cdk activation when translation resumes after release from stress.

A very significant number of proteins belonging to SGs may be phosphorylated by Cdc28 in yeast cells, and, not surprisingly, most of them have functional homologues in mammalian cells (Table S1). The reason Cdc28 would have such a high number of targets in SGs likely resides in their dependence on multivalent protein–protein interactions, which also agrees with the fact that no single protein has been found to be essential for SG formation (Yoon et al., 2010; Yang et al., 2014; Buchan et al., 2013). Intriguingly, a comparative analysis of Cdc28-target phosphosites revealed that their position, rather than being conserved, is very dynamic within disordered regions (Holt et al., 2009).

We show that SG dynamics obey a bistable system where the Cdk is an important effector, and we have recapitulated this behavior with a simple mutual-inhibition model. Notably, the

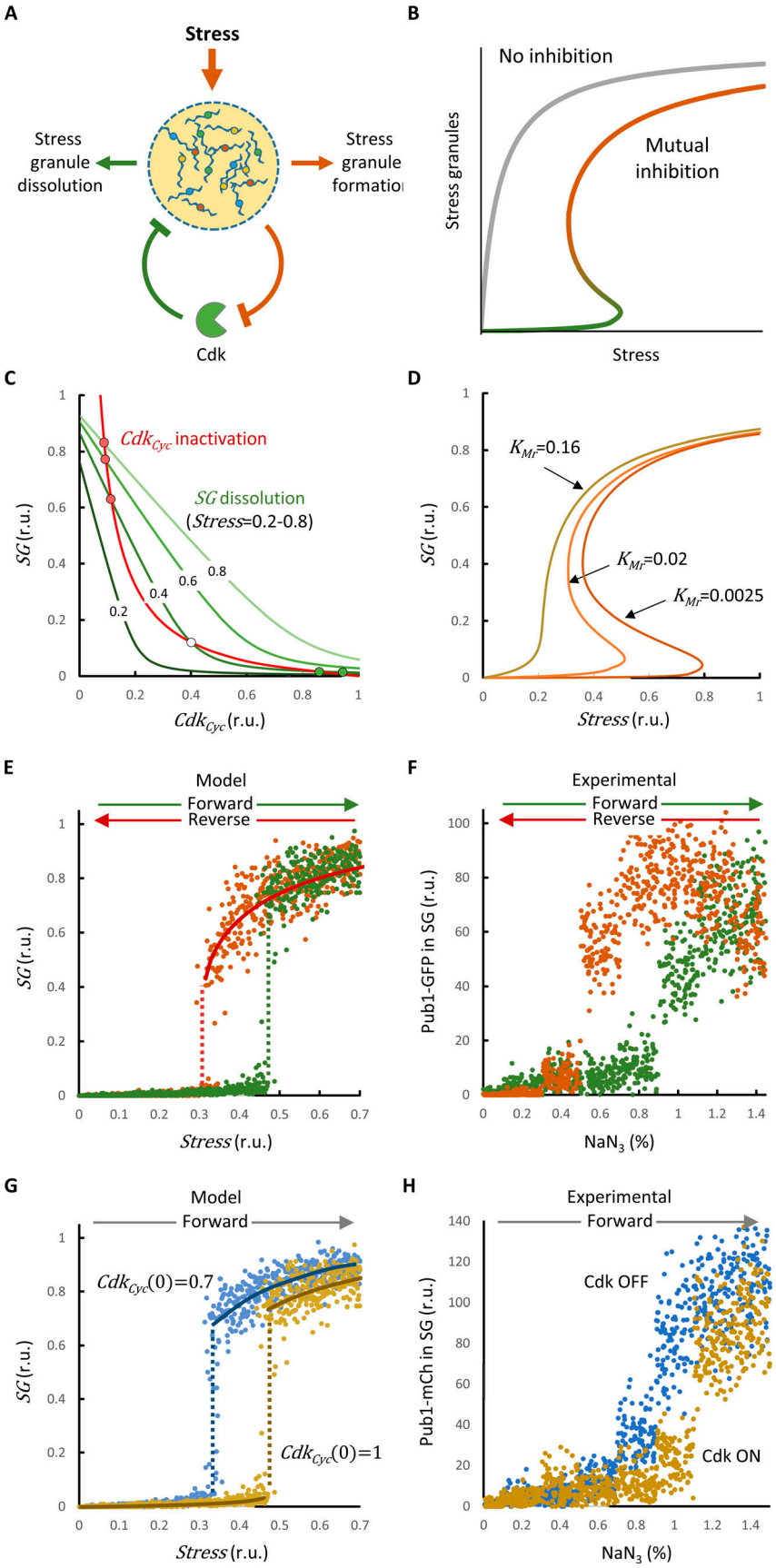

Figure 6. **Mutual inhibition as a bistable system for SG dynamics. (A)** SGs maintain cyclin mRNAs translationally inactive and, hence, inactivate the Cdk. In turn, active Cdk promotes SG dissolution and cyclin mRNA release and translation, thus accelerating SG disassembly. **(B)** SG and Cdk mutual inhibition creates a bistable system that elicits SG formation only above a certain degree of stress and maintains SG integrity until normal conditions are almost fully restored. **(C)** Steady-state balance plots of *SG* and Cdk_{Cyc} as derived from *Stress*-modulated SG dissolution by active Cdk (green lines) or Cdk inactivation by SGs (red line) reactions. Unstable (white circle) and stable (red and green circles) steady states are indicated. **(D)** *SG* steady states versus *Stress* as a function of the K_{Mr}. **(E)** Simulations of *SG* levels in forward or reverse modes. The plot shows final *SG* steady states when the initial *Stress* variable was set to 0 (forward mode, green) or 1 (reverse mode, red), simulating non-stressed and stressed cells, respectively. Both deterministic (lines) and stochastic (dots) simulations are shown. **(F)** SG steady-state levels in forward or reverse mode experiments. In forward mode (green), exponentially growing WT cells expressing Pub1-GFP were subjected to different NaN_3 concentrations for 60 min. In reverse mode, cells were first subjected to 1.4% NaN_3 for 60 min and then incubated in the presence of different NaN_3 concentrations for an additional 60-min period. Pub1-GFP levels in foci were measured in single cells (n > 300), and bootstrapped (n = 50) mean values are plotted. **(G)** Simulations of *SG* levels as a function of the total Cdk levels in forward mode. The plot shows final *SG* steady states when the initial Cdk_{cyc} variable was set to 1 (yellow) or reduced to 0.7 (blue). Both deterministic (lines) and stochastic (dots) simulations are shown. **(H)** SG steady-state levels in forward mode experiments with cycling and G1-arrested cells with no Cdk activity. *GAL1p-CLN3 cln1,2* cells expressing Pub1-mCherry were grown in galactose and arrested in G1 by transfer to glucose for 2 h (Cdk OFF). Then, cells were stressed for 60 min in the presence of different NaN_3 concentrations. As control, *CLN3 cln1,2* cells (Cdk ON) were subjected to the same experimental conditions. Pub1-mCherry levels in foci were measured in single cells (n > 300), and bootstrapped (n = 50) mean values are plotted in relative units (r.u.).

K_M to substrate ratio was crucial to attaining bistability and, if Cdk substrates were always in a soluble form in the cytoplasm, the model would only predict monostable steady-states at varying stress levels. In other words, the higher substrate concentration attained in SGs is what decreases the K_M/substrate ratio and makes the model bistable. Thus, the effects of mutual inhibition would be especially relevant during SG dissolution rather than SG assembly. If this were the case, then SG components would not be necessarily phosphorylated when soluble in the cytoplasm under normal conditions, and, hence, the Cdc28 phosphoproteome could include many other SG proteins in addition to those listed in Table S1. Alternatively, since many SG components display physical interactions even in the absence of stress (Youn et al., 2018), they could interact with Cdc28 in supramolecular complexes to increase their effective concentration as substrates also under nonstress conditions. Favoring the latter possibility, we found that Cdc28 and Whi8 coimmunoprecipitate very efficiently in the absence of stress.

SG dissolution requires the Cdc48 segregase in yeast (Buchan et al., 2013) and mammalian (Wang et al., 2019) cells, and we previously found that Cdc28 phosphorylates Cdc48 to enhance its segregase activity in releasing Cln3 from the ER during G1 (Parisi et al., 2018). Therefore, Cdc28 could also act on SG dissolution by modulating the affinity and/or segregase activity of Cdc48 toward components of the SG.

Giving support to our results, a screen in mammalian cells had pinpointed Cdk inhibitors by their marked effects in delaying SG dissolution (Wippich et al., 2013). These authors identified Dyrk3 as a key factor modulating SG dynamics and recently showed that this kinase is also important for dissolution of specific membraneless organelles during mitosis (Rai et al., 2018). Also in mammalian cells, SG dissolution is modulated by phosphorylation of Grb7 by focal adhesion kinase (Tsai et al., 2008). In yeast, Sky1 is recruited to SGs, where it phosphorylates Npl3 and modulates their dynamics (Shattuck et al., 2019). Therefore, fast and efficient SG assembly and dissolution would result from the concerted action of different protein kinases. Nonetheless, the unique mutual inhibitory roles of Cdk and SGs would provide bistability and hysteresis to prevent SG formation at low levels of stress and sustain their presence until normal conditions are entirely restored. Indeed, as our data suggest, the SG-Cdk mutual inhibitory scenario should also apply to other condensation modulators, thus subjugating SG dynamics to a robust switch as a function of different facets of the cellular physiological status.

Materials and methods

Cells and growth conditions

Yeast strains and plasmids are listed in Table S2 and Table S3, and methods used for chromosomal gene transplacement and PCR-based directed mutagenesis were previously described (Ferrezuelo et al., 2012). Specific construction details will be made available upon request. Unless noted otherwise, all gene fusions in this study were expressed at endogenous levels in yeast cells. Cells were grown for seven or eight generations in SC medium with 2% glucose at 30°C unless stated otherwise. *GAL1*p-driven gene expression was induced by addition of 2% galactose to cultures grown in 2% raffinose at OD_{600} = 0.5 or in the presence of glucose by adding 1 µM β-estradiol to cells expressing the Gal4-hER-VP16 transactivator (Louvion et al., 1993). When indicated, overexpression of *CLN3* was performed with a *tetO*-based expression system (Garí et al., 1997). SG formation was routinely induced by transferring cells to 42°C for 30 min in SC medium without glucose, and SG dissolution was assessed by returning stressed cells to 30°C in SC medium supplemented with glucose. In experiments shown in Fig. 4 F, SG dissolution was assessed at 37°c to maintain restrictive conditions for the thermosensitive *cdc28-13* allele. Finally, SG steady states were analyzed by treating cells with the indicated concentrations of NaN_3 for 60 min at 30°C in SC plus 1% glucose.

Human HeLa and U2OS cells were grown at 37°C in DMEM supplemented with glutamine, antibiotics, and 10% FBS. Transfection with Caprin1-directed (TRCN0000115972) or control (SHC002) shRNAs and vectors expressing NLS-MCP-GFP, 3HA-Cdk4, $Geminin_{1–110}$-mVenus or mCherry-G3BP1 proteins, or *CCND1-MS2* mRNA was performed as described previously (Ruiz-Miró et al., 2011). Cycling cells were analyzed 18 h after replating, and SG formation was induced by addition of 0.5 mM $NaAsO_2$ for 30 min, unless stated otherwise. SG steady states were analyzed after 60 min in $NaAsO_2$ at the indicated concentrations.

Subcellular fractionation

Briefly, cells (50 OD_{600}) were pelleted and disrupted with glass beads in 200 µl STE10 (10% sucrose, 10 mM Tris-HCl, pH 7.6, and 10 mM EDTA) with protease inhibitors (Vergés et al., 2007). Cleared extracts were layered on top of a 5-ml, 20–60% linear sucrose gradient, and centrifuged for 18 h at 100,000 *g* in a SW50.1 rotor (Beckman Coulter). Fractions (0.5 ml) were collected from the top of the gradient, precipitated with 7% trichloroacetic acid, and analyzed by immunoblotting as described below.

Immunoprecipitation

Cells (50 OD_{600}) were disrupted with glass beads in 200 µl BFI buffer (0.1% Triton X-100, 250 mM NaCl, 50 mM Tris-HCl, pH 7.5, and 5 mM EDTA) with protease inhibitors (Wang et al., 2004). Cleared lysates were incubated with 30 µl αFLAG (clone M2; Sigma) beads, which, after three washing steps, were boiled briefly in 2x loading buffer before SDS-PAGE.

Immunoblot and immunofluorescence analysis

Immunoblotting was performed essentially as described previously (Gallego et al., 1997). Protein gels were transferred to nitrocellulose and probed with primary and secondary antibodies as recommended by the supplier in PBS. Immunofluorescence analysis in yeast (Wang et al., 2004) and HeLa (Ruiz-Miró et al., 2011) cells were performed as described. Used antibodies are listed in Table S4.

mRNA quantification by quantitative RT-PCR

Cells (10 OD_{600}) were disrupted with glass beads in 50 µl of 1:1 phenol/Tris/ethylenediaminetetraacetate, and total RNA was

precipitated with ethanol in the presence of 0.3M NaOAc pH 5.2. Determination of mRNA levels by quantitative RT-PCR was done using probes listed in Table S5.

Time-lapse wide-field and confocal microscopy

Yeast cells were analyzed by wide-field epifluorescence microscopy in 35-mm glass-bottom culture dishes (GWST-3522; WillCo) in SC media at 30°C essentially as described previously (Ferrezuelo et al., 2012) using a fully motorized Leica AF7000 microscope with a HCX PL S-APO 63×/1.3-NA oil-immersion objective at room temperature, equipped with a digital charge-coupled device camera ORCA-R2. Wide-field images were analyzed with the aid of BudJ, an ImageJ (Wayne Rasband, National Institutes of Health) plugin to obtain cell dimensions and fluorescence data as described previously (Ferrezuelo et al., 2012). Intracellular foci were detected with BudJ as pixels with a fluorescence value above a certain threshold relative to the median cell fluorescence that produced a contiguous area with a minimum size (both set by the user). In a typical setup, pixels were selected if at least 30% brighter than the cell median, with a minimal size of 0.2 µm. Photobleaching during acquisition was negligible (less than 0.1% per time point), and autofluorescence was always subtracted. Immunofluorescence in mammalian cells was analyzed under a Zeiss 780 confocal microscope with a C-Apochromat 40×/1.2NA water-immersion objective. Time lapse of U2OS cells was performed as for yeast cells in DMEM supplemented with glutamine and 10% FBS at 37°C in 5% CO_2. Intracellular foci were analyzed as abovementioned with a plugin derived from BudJ adapted to images from cultured mammalian cells.

Mutual-inhibition mathematical model

A wiring diagram and a set of differential equations were produced with the aid of COPASI (Hoops et al., 2006) to describe the mutual-inhibition framework (Fig. S5 A). First, we considered SG factors as either free components (SG_{Comp}) or in a condensed state (SG), the stress signal ($Stress$) acting as a positive modulator in their condensation. Regarding SG dissolution, we assumed two independent mechanisms, a basal process that reverses condensation in the absence of stress and a Cdk-dependent dissolution reaction in which active Cdk (Cdk_{Cyc}) acts as an enzyme with specific catalytic (k_c) and Michaelis-Menten (K_M) constants. In turn, active Cdk (Cdk_{Cyc}) is inactivated (Cdk) as a function of condensed SG factors (SG) to simulate translation inhibition of G1 cyclin mRNAs by SGs. Finally, we assumed stress-independent reactivation kinetics of the Cdk. With the exception of Cdk-dependent SG dissolution, all processes were defined by mass-action laws with explicit rate constants. This simplicity allowed us to estimate all kinetic parameters from experimental data using COPASI in deterministic mode. First, the K_M for Cdc28 was previously determined in vitro (Bouchoux and Uhlmann, 2011), and the maximal substrate concentration in SGs (SG_{max}) was estimated as described in Fig. S5 B, allowing us to obtain a relative $K_{Mr} = K_M/SG_{max}$. We obtained the basal SG-dissolution rate constant (k_{bd}) by fitting the model to SG dissolution in the *cdc28-13* mutant in the absence of stress (Fig. S5 C), where all other variables have no effect. We then used SG formation and dissolution data from WT cells to estimate the remaining rate constants (Fig. S5 D).

Statistical analysis

Sample size is always indicated in the figure legend. For single-cell or single-focus data, median and quartile (Q) values are shown. Confidence limits for the median were obtained by bootstrapping-based methods. Pairwise comparisons were performed with a Mann–Whitney *U* test, and the resulting P values are shown in the corresponding figure panels. Time-lapse data from single cells during SG formation or dissolution are represented as the mean value of the population along time, while the shaded area represents the 95% confidence limits of the mean. Protein and mRNA levels were determined in triplicate samples, and mean + SEM values are shown. Venn diagrams were as described previously (Heberle et al., 2015).

Data and software availability

The model was deposited in the BioModels (Chelliah et al., 2015) database as MODEL2003140002 in SBML format together with a COPASI (Hoops et al., 2006) file to reproduce simulations with the parameter set shown in Fig. S5. BudJ (Ferrezuelo et al., 2012) can be obtained as an ImageJ (Wayne Rasband, National Institutes of Health) plugin from ibmb.csic.es/groups/spatial-control-of-cell-cycle-entry.

Online supplemental material

Fig. S1 contains control data and representative images related to the localization of the *CLN3* mRNA in SGs. Fig. S2 shows Cln3 protein levels by immunoblotting during stress as a function of Whi8, as well as effects of Whi8 on nuclear Cln3 levels by immunofluorescence. Fig. S3 displays representative images of Cdc28 recruited to SGs under stress as a function of Whi8, the effects of cell cycle position and Cln3 overexpression in SG-dissolution dynamics, and levels of a set of SG-recruited mRNAs as GFP fusions. Fig. S4 contains representative images showing the colocalization of the cyclin D1 mRNA with TIA1 in SGs and levels of cyclin D1 protein and mRNA during stress. Fig. S5 shows the equations and parameter fitting steps used to setup the mutual-inhibition model described in Fig. 6. Table S1 lists the putative Cdc28 phosphorylation targets in SGs. Table S2 lists yeast strains used in this study. Table S3 lists plasmids used in this study. Table S4 lists antibodies used in this study. Table S5 lists qRT-PCR probes used in this study.

Acknowledgments

We thank E. Rebollo for technical assistance and B. Futcher (State University of New York at Stony Brook, Stony Brook, NY), R. Singer (Albert Einstein College of Medicine, New York, NY) and T. Stracker (Institute for Biomedical Research, Barcelona, Spain) for providing strains, cell lines, and plasmids. We also thank C. Rose for editing the manuscript.

This work was funded by the Spanish Ministry of Science and Innovation and the European Union (FEDER; grant BFU2017-83375-R to C. Gallego and grant BFU2016-80234-R to M. Aldea).

A.P. Pérez and D.F. Moreno received Generalitat de Catalunya FI fellowships.

The authors declare no competing financial interests.

Author contributions: Investigation and Methodology, G. Yahya; Investigation, A.P. Pérez, M.B. Mendoza, E. Parisi, D.F. Moreno, and M. Artés; Conceptualization, Supervision, Funding Acquisition, Investigation and Writing — Original Draft and Review & Editing, C. Gallego; Conceptualization, Supervision, Funding Acquisition, Investigation and Writing — Original Draft and Review & Editing, M. Aldea.

Submitted: 13 May 2020
Revised: 27 November 2020
Accepted: 23 December 2020

References

Alberti, S., and D. Dormann. 2019. Liquid–liquid phase separation in disease. *Annu. Rev. Genet.* 53:171–194. https://doi.org/10.1146/annurev-genet-112618-043527

Alberti, S., A. Gladfelter, and T. Mittag. 2019. Considerations and challenges in studying liquid-liquid phase separation and biomolecular condensates. *Cell.* 176:419–434. https://doi.org/10.1016/j.cell.2018.12.035

Banani, S.F., H.O. Lee, A.A. Hyman, and M.K. Rosen. 2017. Biomolecular condensates: organizers of cellular biochemistry. *Nat. Rev. Mol. Cell Biol.* 18:285–298. https://doi.org/10.1038/nrm.2017.7

Bellí, G., E. Garí, M. Aldea, and E. Herrero. 2001. Osmotic stress causes a G1 cell cycle delay and downregulation of Cln3/Cdc28 activity in Saccharomyces cerevisiae. *Mol. Microbiol.* 39:1022–1035. https://doi.org/10.1046/j.1365-2958.2001.02297.x

Bouchoux, C., and F. Uhlmann. 2011. A quantitative model for ordered Cdk substrate dephosphorylation during mitotic exit. *Cell.* 147:803–814. https://doi.org/10.1016/j.cell.2011.09.047

Bratek-Skicki, A., R. Pancsa, B. Meszaros, J. Van Lindt, and P. Tompa. 2020. A guide to regulation of the formation of biomolecular condensates. *FEBS J.* 287:1924–1935. https://doi.org/10.1111/febs.15254

Buchan, J.R., D. Muhlrad, and R. Parker. 2008. P bodies promote stress granule assembly in Saccharomyces cerevisiae. *J. Cell Biol.* 183:441–455. https://doi.org/10.1083/jcb.200807043

Buchan, J.R., R.M. Kolaitis, J.P. Taylor, and R. Parker. 2013. Eukaryotic stress granules are cleared by autophagy and Cdc48/VCP function. *Cell.* 153:1461–1474. https://doi.org/10.1016/j.cell.2013.05.037

Cai, Y., and B. Futcher. 2013. Effects of the yeast RNA-binding protein Whi3 on the half-life and abundance of CLN3 mRNA and other targets. *PLoS One.* 8:e84630. https://doi.org/10.1371/journal.pone.0084630

Chelliah, V., N. Juty, I. Ajmera, R. Ali, M. Dumousseau, M. Glont, M. Hucka, G. Jalowicki, S. Keating, V. Knight-Schrijver, et al. 2015. BioModels: ten-year anniversary. *Nucleic Acids Res.* 43(D1):D542–D548. https://doi.org/10.1093/nar/gku1181

Colomina, N., F. Ferrezuelo, H. Wang, M. Aldea, and E. Garí. 2008. Whi3, a developmental regulator of budding yeast, binds a large set of mRNAs functionally related to the endoplasmic reticulum. *J. Biol. Chem.* 283:28670–28679. https://doi.org/10.1074/jbc.M804604200

Crawford, R.A., and G.D. Pavitt. 2019. Translational regulation in response to stress in Saccharomyces cerevisiae. *Yeast.* 36:5–21. https://doi.org/10.1002/yea.3349

de Nadal, E., G. Ammerer, and F. Posas. 2011. Controlling gene expression in response to stress. *Nat. Rev. Genet.* 12:833–845. https://doi.org/10.1038/nrg3055

Ferrezuelo, F., N. Colomina, A. Palmisano, E. Garí, C. Gallego, A. Csikász-Nagy, and M. Aldea. 2012. The critical size is set at a single-cell level by growth rate to attain homeostasis and adaptation. *Nat. Commun.* 3:1012. https://doi.org/10.1038/ncomms2015

Gallego, C., E. Garí, N. Colomina, E. Herrero, and M. Aldea. 1997. The Cln3 cyclin is down-regulated by translational repression and degradation during the G1 arrest caused by nitrogen deprivation in budding yeast. *EMBO J.* 16:7196–7206. https://doi.org/10.1093/emboj/16.23.7196

Garí, E., L. Piedrafita, M. Aldea, and E. Herrero. 1997. A set of vectors with a tetracycline-regulatable promoter system for modulated gene expression in Saccharomyces cerevisiae. *Yeast.* 13:837–848. https://doi.org/10.1002/(SICI)1097-0061(199707)13:9<837::AID-YEA145>3.0.CO;2-T

Garí, E., T. Volpe, H. Wang, C. Gallego, B. Futcher, and M. Aldea. 2001. Whi3 binds the mRNA of the G1 cyclin CLN3 to modulate cell fate in budding yeast. *Genes Dev.* 15:2803–2808. https://doi.org/10.1101/gad.203501

González-Novo, A., J. Jiménez, J. Clotet, M. Nadal-Ribelles, S. Cavero, E. de Nadal, and F. Posas. 2015. Hog1 targets Whi5 and Msa1 transcription factors to downregulate cyclin expression upon stress. *Mol. Cell. Biol.* 35:1606–1618. https://doi.org/10.1128/MCB.01279-14

Heberle, H., G.V. Meirelles, F.R. da Silva, G.P. Telles, and R. Minghim. 2015. InteractiVenn: a web-based tool for the analysis of sets through Venn diagrams. *BMC Bioinformatics.* 16:169. https://doi.org/10.1186/s12859-015-0611-3

Ho, B., A. Baryshnikova, and G.W. Brown. 2018. Unification of Protein Abundance Datasets Yields a Quantitative Saccharomyces cerevisiae Proteome. *Cell Syst.* 6:192–205.e3. https://doi.org/10.1016/j.cels.2017.12.004

Holmes, K.J., D.M. Klass, E.L. Guiney, and M.S. Cyert. 2013. Whi3, an S. cerevisiae RNA-binding protein, is a component of stress granules that regulates levels of its target mRNAs. *PLoS One.* 8:e84060. https://doi.org/10.1371/journal.pone.0084060

Holt, L.J., B.B. Tuch, J. Villén, A.D. Johnson, S.P. Gygi, and D.O. Morgan. 2009. Global analysis of Cdk1 substrate phosphorylation sites provides insights into evolution. *Science.* 325:1682–1686. https://doi.org/10.1126/science.1172867

Hoops, S., S. Sahle, R. Gauges, C. Lee, J. Pahle, N. Simus, M. Singhal, L. Xu, P. Mendes, and U. Kummer. 2006. COPASI–a complex pathway simulator. *Bioinformatics.* 22:3067–3074. https://doi.org/10.1093/bioinformatics/btl485

Huh, W.-K., J.V. Falvo, L.C. Gerke, A.S. Carroll, R.W. Howson, J.S. Weissman, and E.K. O'Shea. 2003. Global analysis of protein localization in budding yeast. *Nature.* 425:686–691. https://doi.org/10.1038/nature02026

Jain, S., J.R. Wheeler, R.W. Walters, A. Agrawal, A. Barsic, and R. Parker. 2016. ATPase-modulated stress granules contain a diverse proteome and substructure. *Cell.* 164:487–498. https://doi.org/10.1016/j.cell.2015.12.038

Kedersha, N., and P. Anderson. 2007. Mammalian stress granules and processing bodies. *Methods Enzymol.* 431:61–81. https://doi.org/10.1016/S0076-6879(07)31005-7

Kedersha, N., M.D. Panas, C.A. Achorn, S. Lyons, S. Tisdale, T. Hickman, M. Thomas, J. Lieberman, G.M. McInerney, P. Ivanov, and P. Anderson. 2016. G3BP-Caprin1-USP10 complexes mediate stress granule condensation and associate with 40S subunits. *J. Cell Biol.* 212:845–860. https://doi.org/10.1083/jcb.201508028

Khong, A., T. Matheny, S. Jain, S.F. Mitchell, J.R. Wheeler, and R. Parker. 2017. The stress granule transcriptome reveals principles of mRNA accumulation in stress granules. *Mol. Cell.* 68:808–820.e5. https://doi.org/10.1016/j.molcel.2017.10.015

Kojima, R., S. Kajiura, H. Sesaki, T. Endo, and Y. Tamura. 2016. Identification of multi-copy suppressors for endoplasmic reticulum-mitochondria tethering proteins in Saccharomyces cerevisiae. *FEBS Lett.* 590:3061–3070. https://doi.org/10.1002/1873-3468.12358

Louvion, J.F., B. Havaux-Copf, and D. Picard. 1993. Fusion of GAL4-VP16 to a steroid-binding domain provides a tool for gratuitous induction of galactose-responsive genes in yeast. *Gene.* 131:129–134. https://doi.org/10.1016/0378-1119(93)90681-R

Moreno, D.F., E. Parisi, G. Yahya, F. Vaggi, A. Csikász-Nagy, and M. Aldea. 2019. Competition in the chaperone-client network subordinates cell-cycle entry to growth and stress. *Life Sci. Alliance.* 2:e201800277. https://doi.org/10.26508/lsa.201800277

Namkoong, S., A. Ho, Y.M. Woo, H. Kwak, and J.H. Lee. 2018. Systematic characterization of stress-induced RNA granulation. *Mol. Cell.* 70:175–187.e8. https://doi.org/10.1016/j.molcel.2018.02.025

Parisi, E., G. Yahya, A. Flores, and M. Aldea. 2018. Cdc48 / p97 segregase is modulated by Cdk to determine cyclin fate during G1 progression. *EMBO J.* 37:e98724. https://doi.org/10.15252/embj.201798724

Protter, D.S.W., and R. Parker. 2016. Principles and properties of stress granules. *Trends Cell Biol.* 26:668–679. https://doi.org/10.1016/j.tcb.2016.05.004

Rai, A.K., J.X. Chen, M. Selbach, and L. Pelkmans. 2018. Kinase-controlled phase transition of membraneless organelles in mitosis. *Nature.* 559:211–216. https://doi.org/10.1038/s41586-018-0279-8

Rowley, A., G.C. Johnston, B. Butler, M. Werner-Washburne, and R.A. Singer. 1993. Heat shock-mediated cell cycle blockage and G1 cyclin expression

in the yeast Saccharomyces cerevisiae. *Mol. Cell. Biol.* 13:1034–1041. https://doi.org/10.1128/MCB.13.2.1034

Ruiz-Miró, M., N. Colomina, R.M.H. Fernández, E. Garí, C. Gallego, and M. Aldea. 2011. Translokin (Cep57) interacts with cyclin D1 and prevents its nuclear accumulation in quiescent fibroblasts. *Traffic.* 12:549–562. https://doi.org/10.1111/j.1600-0854.2011.01176.x

Shah, K.H., R. Nostramo, B. Zhang, S.N. Varia, B.M. Klett, and P.K. Herman. 2014. Protein kinases are associated with multiple, distinct cytoplasmic granules in quiescent yeast cells. *Genetics.* 198:1495–1512. https://doi.org/10.1534/genetics.114.172031

Shattuck, J.E., K.R. Paul, S.M. Cascarina, and E.D. Ross. 2019. The prion-like protein kinase Sky1 is required for efficient stress granule disassembly. *Nat. Commun.* 10:3614. https://doi.org/10.1038/s41467-019-11550-w

Shin, Y., and C.P. Brangwynne. 2017. Liquid phase condensation in cell physiology and disease. *Science.* 357:eaaf4382. doi:. https://doi.org/10.1126/science.aaf4382

Siwiak, M., and P. Zielenkiewicz. 2010. A comprehensive, quantitative, and genome-wide model of translation. *PLOS Comput. Biol.* 6:e1000865. https://doi.org/10.1371/journal.pcbi.1000865

Snead, W.T., and A.S. Gladfelter. 2019. The control centers of biomolecular phase separation: how membrane surfaces, PTMs, and active processes regulate condensation. *Mol. Cell.* 76:295–305. https://doi.org/10.1016/j.molcel.2019.09.016

Solé, C., M. Nadal-Ribelles, E. de Nadal, and F. Posas. 2015. A novel role for lncRNAs in cell cycle control during stress adaptation. *Curr. Genet.* 61:299–308. https://doi.org/10.1007/s00294-014-0453-y

Solomon, S., Y. Xu, B. Wang, M.D. David, P. Schubert, D. Kennedy, and J.W. Schrader. 2007. Distinct structural features of caprin-1 mediate its interaction with G3BP-1 and its induction of phosphorylation of eukaryotic translation initiation factor 2alpha, entry to cytoplasmic stress granules, and selective interaction with a subset of mRNAs. *Mol. Cell. Biol.* 27:2324–2342. https://doi.org/10.1128/MCB.02300-06

Tsai, N.-P., P.-C. Ho, and L.-N. Wei. 2008. Regulation of stress granule dynamics by Grb7 and FAK signalling pathway. *EMBO J.* 27:715–726. https://doi.org/10.1038/emboj.2008.19

Tutucci, E., M. Vera, J. Biswas, J. Garcia, R. Parker, and R.H. Singer. 2018. An improved MS2 system for accurate reporting of the mRNA life cycle. *Nat. Methods.* 15:81–89. https://doi.org/10.1038/nmeth.4502

Vai, M., L. Popolo, and L. Alberghina. 1987. Effect of tunicamycin on cell cycle progression in budding yeast. *Exp. Cell Res.* 171:448–459. https://doi.org/10.1016/0014-4827(87)90176-5

Van Treeck, B., D.S.W. Protter, T. Matheny, A. Khong, C.D. Link, and R. Parker. 2018. RNA self-assembly contributes to stress granule formation and defining the stress granule transcriptome. *Proc. Natl. Acad. Sci. USA.* 115:2734–2739. https://doi.org/10.1073/pnas.1800038115

Vergés, E., N. Colomina, E. Garí, C. Gallego, and M. Aldea. 2007. Cyclin Cln3 is retained at the ER and released by the J chaperone Ydj1 in late G1 to trigger cell cycle entry. *Mol. Cell.* 26:649–662. https://doi.org/10.1016/j.molcel.2007.04.023

Wang, H., E. Garí, E. Vergés, C. Gallego, and M. Aldea. 2004. Recruitment of Cdc28 by Whi3 restricts nuclear accumulation of the G1 cyclin-Cdk complex to late G1. *EMBO J.* 23:180–190. https://doi.org/10.1038/sj.emboj.7600022

Wang, B., B.A. Maxwell, J.H. Joo, Y. Gwon, J. Messing, A. Mishra, T.I. Shaw, A.L. Ward, H. Quan, S.M. Sakurada, et al. 2019. ULK1 and ULK2 regulate stress Granule disassembly through phosphorylation and activation of VCP/p97. *Mol. Cell.* 74:742–757.e8. https://doi.org/10.1016/j.molcel.2019.03.027

Wippich, F., B. Bodenmiller, M.G. Trajkovska, S. Wanka, R. Aebersold, and L. Pelkmans. 2013. Dual specificity kinase DYRK3 couples stress granule condensation/dissolution to mTORC1 signaling. *Cell.* 152:791–805. https://doi.org/10.1016/j.cell.2013.01.033

Yahya, G., E. Parisi, A. Flores, C. Gallego, and M. Aldea. 2014. A Whi7-anchored loop controls the G1 Cdk-cyclin complex at start. *Mol. Cell.* 53:115–126. https://doi.org/10.1016/j.molcel.2013.11.015

Yang, X., Y. Shen, E. Garre, X. Hao, D. Krumlinde, M. Cvijović, C. Arens, T. Nyström, B. Liu, and P. Sunnerhagen. 2014. Stress granule-defective mutants deregulate stress responsive transcripts. *PLoS Genet.* 10:e1004763. https://doi.org/10.1371/journal.pgen.1004763

Yoon, J.-H., E.-J. Choi, and R. Parker. 2010. Dcp2 phosphorylation by Ste20 modulates stress granule assembly and mRNA decay in Saccharomyces cerevisiae. *J. Cell Biol.* 189:813–827. https://doi.org/tlsb

Youn, J.-Y.Y., W.H. Dunham, S.J. Hong, J.D.R. Knight, M. Bashkurov, G.I. Chen, H. Bagci, B. Rathod, G. MacLeod, S.W.M. Eng, et al. 2018. High-density proximity mapping reveals the subcellular organization of mRNA-associated granules and bodies. *Mol. Cell.* 69:517–532.e11. https://doi.org/10.1016/j.molcel.2017.12.020

JCB

Supplemental material

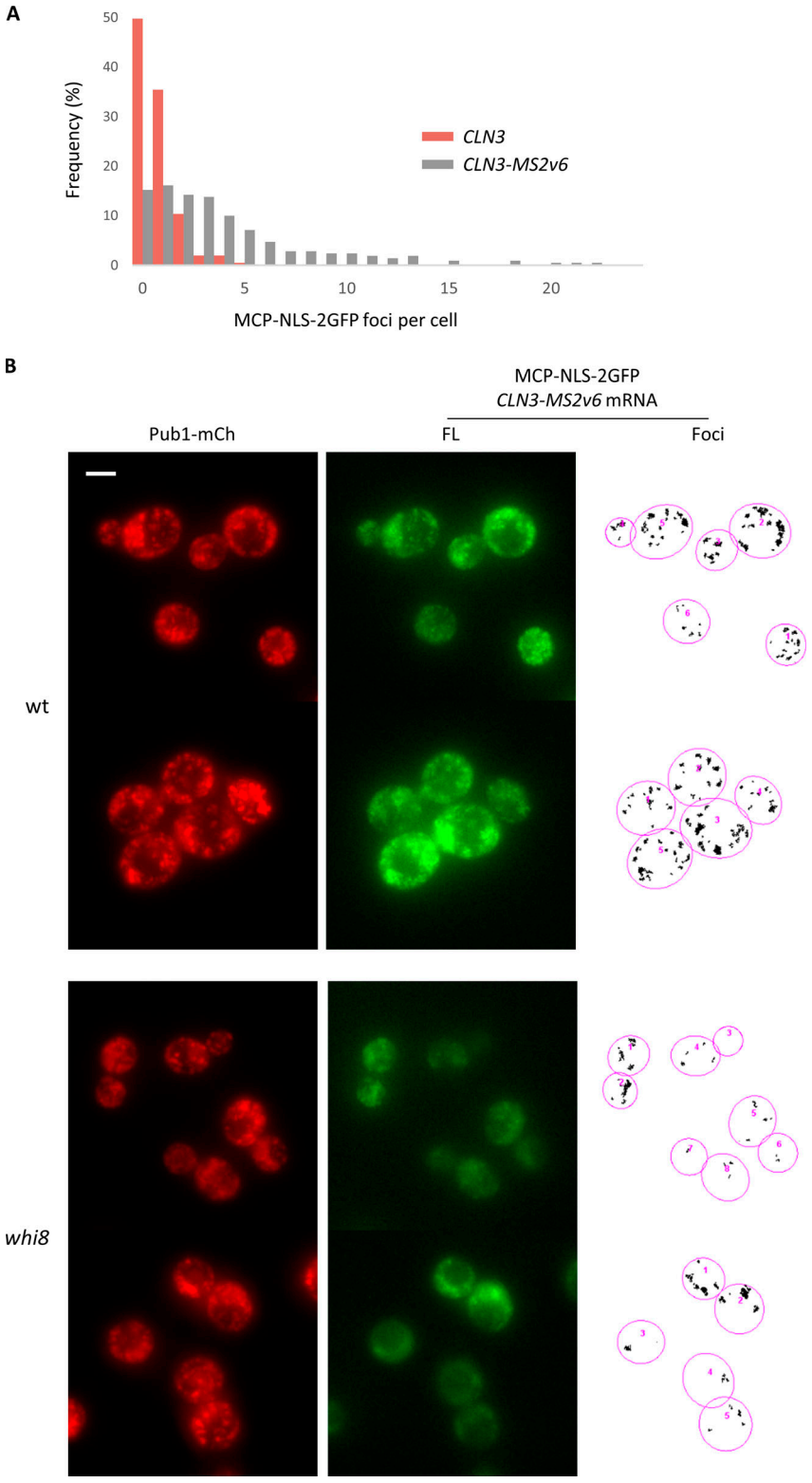

Figure S1. **Whi8 binds and recruits the *CLN3* mRNA to SGs. (A)** *MCP-NLS-GFP* foci numbers in *WHI8-mCh* cells (n = 200) with plasmids expressing either *CLN3* or *CLN3-MS2v6* after 30 min at 42°C in the absence of glucose. **(B)** *PUB1-mCh* cells with the indicated genotypes with plasmids expressing *MCP-NLS-GFP* and *CLN3-MS2v6* were stressed for 30 min at 42°C in the absence of glucose. Foci detected above a fixed local threshold with the aid of BudJ are also shown. Scale bar, 2 µm. wt, wild type.

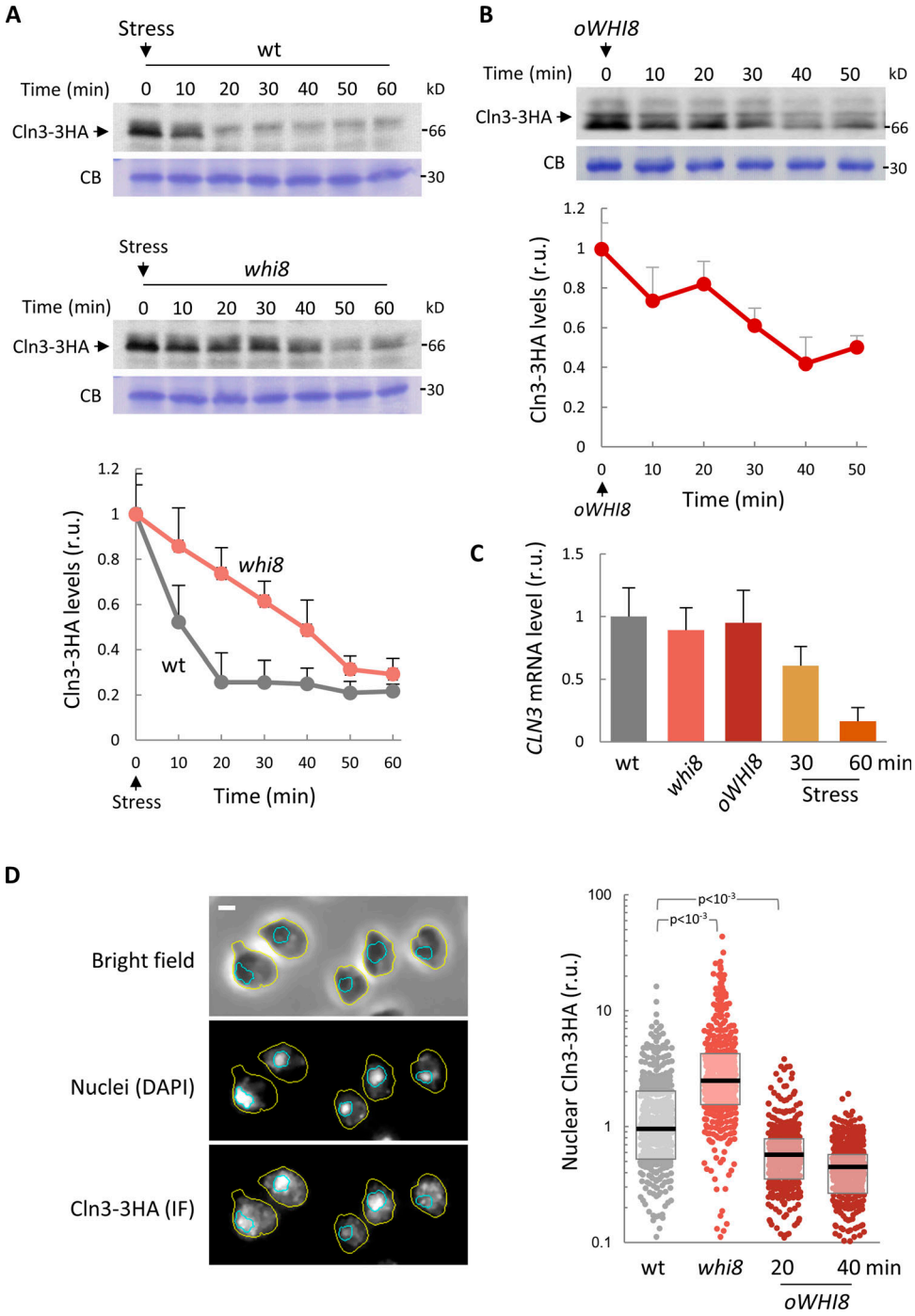

Figure S2. **Whi8 is required to inhibit *CLN3* mRNA translation under stress conditions. (A)** Immunoblot analysis of Cln3-3HA after transferring WT (top) or *whi8* (bottom) cells to 42°C in the absence of glucose. Total cell extracts were stained with Coomassie blue, and a prominent band is shown as a loading control. Cln3-3HA levels were quantified, and mean + SEM values (n = 3) are plotted. **(B)** Immunoblot analysis of Cln3-3HA after 1 µM β-estradiol addition to induce a plasmid-borne *GAL1p-WHI8* fusion in cells expressing the Gal4-hER-VP16 transactivator. A prominent band in the total cell extract is shown as loading control. Cln3-3HA levels were quantified, and mean + SEM values (n = 3) are plotted. **(C)** *CLN3* mRNA levels were determined in cells of the indicated genotypes under normal conditions or 30–60 min after transfer to 42°C in the absence of glucose. Mean + SEM values (n = 3) are plotted. **(D)** Cells with the indicated genotypes were analyzed to determine Cln3-3HA nuclear levels by immunofluorescence (left; Vergés et al., 2007). Scale bar, 2 µm. Individual data (n > 400) and median ± Q values are plotted (right) in relative units (r.u.). Shown P values were obtained using a Mann–Whitney U test. wt, wild type.

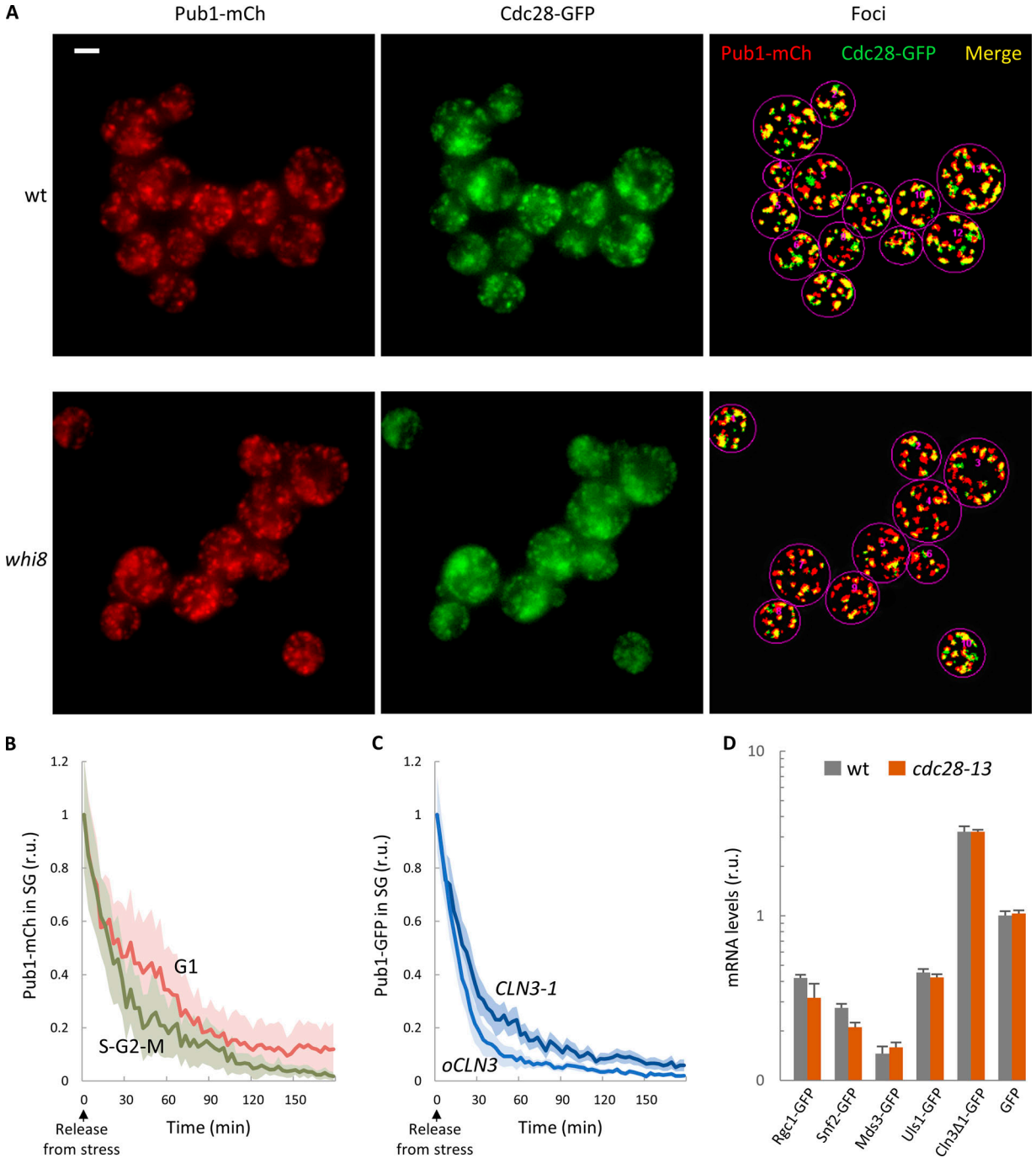

Figure S3. **Cdc28 is recruited to SGs and modulates SG dynamics. (A)** Maximum projections of confocal images from WT and *whi8* cells expressing Cdc8-GFP and Pub1-mCherry after 30 min at 42°C in the absence of glucose. Scale bar, 2 µm. **(B)** WT cells expressing Pub1-mCherry were stressed for 30 min at 42°C in the absence of glucose, and, once released at 30°C in the presence of glucose, Pub1-mCherry levels in foci were measured at different time points in unbudded (G1) or budded (S-G2-M) cells. Mean values (n > 30) and confidence limits for the mean (α = 0.05) are plotted. **(C)** *PUB1-mCh* cells with plasmids expressing a hyperstable allele (*CLN3-1*) or overexpressing WT Cln3 (*oCLN3*) from the *tetO*$_2$ promoter were stressed for 30 min at 42°C in the absence of glucose and, once released at 30°C in the presence of glucose, Pub1-mCherry levels in foci were measured at different time points. Mean values (n > 30) and confidence limits for the mean (α = 0.05) are plotted. **(D)** WT (gray) and *cdc28-13* (orange) cells with plasmids expressing the indicated GFP fusions as in Fig. 4 J were collected 100 min after release from stress, and mRNA levels were analyzed by RT-PCR. Mean (n = 3) and standard error values are plotted in relative units (r.u.). wt, wild type.

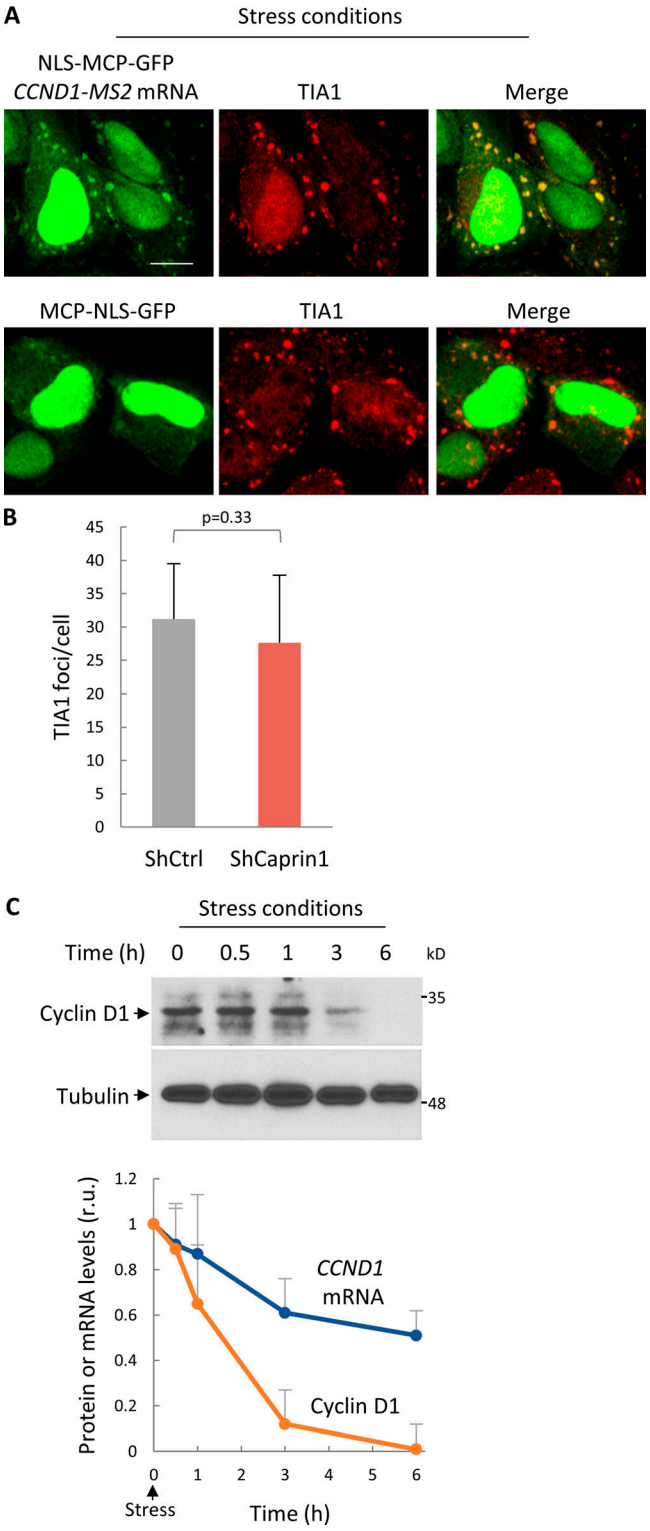

Figure S4. **The *CCND1* mRNA is recruited to SGs and cyclin D1 levels are down-regulated by stress. (A)** HeLa cells with plasmids expressing NLS-MCP-GFP and *CCND1-MS2* mRNA or only NLS-MCP-GFP as control were subjected to 0.5 mM $NaAsO_2$ for 30 min and analyzed by immunofluorescence with a αTIA1 antibody. Scale bar, 5 µm. **(B)** HeLa cells with plasmids expressing either shCaprin1 or shCtrl were subjected to 0.5 mM $NaAsO_2$ for 30 min, and the number of TIA1 foci per cell was determined by immunofluorescence as in A. Mean (n = 100, α = 0.05) values and confidence limits for the mean are plotted. **(C)** Immunoblot analysis of cyclin D1 in HeLa cells at the indicated times after addition of 0.5 mM $NaAsO_2$. Tubulin is shown as a loading control. Cyclin D1 protein and *CCND1* mRNA levels were quantified, and mean + SEM values (n = 3) are plotted in relative units (r.u.).

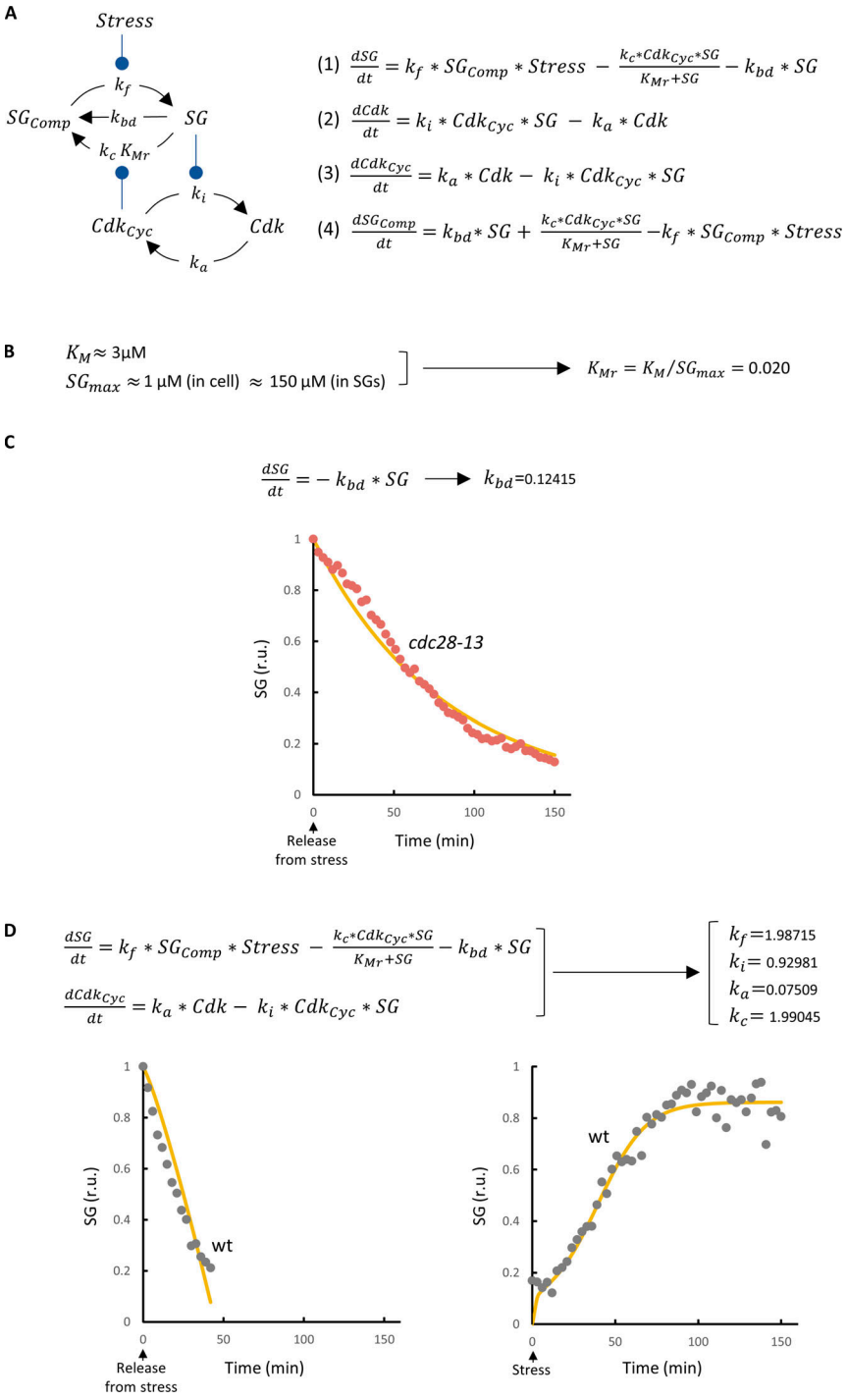

Figure S5. **Equations and parameter fitting in the mutual-inhibition model. (A)** Wire diagram of the mutual-inhibition model opposing SG formation and Cdk activity. Variables and parameters used in the model are indicated. This model has four state variables: SG_{Comp}, SG free components; SG, SG condensed factors; Cdk_{Cyc}, active Cdk-cyclin complexes; and Cdk, inactive Cdk molecules. With the exception of SG dissolution by Cdk, all reactions are driven by simple mass-action laws with explicit parameters. Stress acts on SG formation by modulating condensation of SG components with k_f, the formation rate constant. SG dissolution, in turn, takes place through (1) a default basal process with rate constant k_{bd}, and (2) a Cdk-mediated enzymatic mechanism with k_c (catalytic constant) and K_{Mr} (relative Michaelis-Menten constant) parameters. Cdk is activated at a constant rate (k_a) and, as cyclin mRNA becomes translationally inhibited, is down-regulated by SGs with an inactivation constant k_i. The set of nonlinear differential equations used to simulate the model is also shown. **(B)** Cdc28 has a mean K_M of ∼3 μM (Bouchoux and Uhlmann, 2011), and putative Cdc28 targets in SGs (Table S1) display an average concentration close to 1 μM (Ho et al., 2018). We carefully analyzed Whi8-GFP and Pub1-GFP levels (as in Fig. 4 A) estimated that these proteins increase their concentration by ∼150-fold in SGs under stress conditions. Thus, $K_{Mr} = K_M/SG_{max}$ is ∼0.02. **(C)** The basal SG-dissolution rate constant (k_{bd}) was obtained by fitting the model to SG dissolution in the *cdc28-13* mutant in the absence of stress, where all other variables have no effect. Equations used and the resulting fitted curve (yellow line) are shown. **(D)** The remaining parameters of the model were obtained by fitting the model to SG formation and dissolution experimental data (gray points) in relative units (r.u.) from WT cells. Equations used and the resulting fitted curves (yellow lines) are shown. wt, wild type.

Tables S1–S5 are provided online. Table S1 lists Cdc28 targets in SGs. Table S2 lists yeast strains used in this study. Table S3 lists plasmids used in this study. Table S4 lists antibodies used in this study. Table S5 lists qRT-PCR probes used in this study.